A transient role of the ciliary gene Inpp5e in controlling direct versus indirect neurogenesis in cortical development

A transient role of the ciliary gene *Inpp5e* in controlling direct versus indirect neurogenesis in cortical development

Kerstin Hasenpusch-Theil[1,2], Christine Laclef[3,4], Matt Colligan[1], Eamon Fitzgerald[1], Katherine Howe[1], Emily Carroll[1], Shaun R. Abrams[5], Jeremy F. Reiter[5,6], Sylvie Schneider-Maunoury[3], and Thomas Theil[1,2,7]

[1]Centre for Discovery Brain Sciences, Hugh Robson Building, University of Edinburgh, Edinburgh, EH8 9XD, United Kingdom

[2]Simons Initiative for the Developing Brain, University of Edinburgh, Hugh Robson Building, Edinburgh, EH8 9XD, United Kingdom

[3]Sorbonne Université, CNRS UMR7622, INSERM U1156, Institut de Biologie Paris Seine (IBPS) - Developmental Biology Unit, 75005, Paris, France

[4]Present address: Sorbonne Université, Institut du Fer à Moulin INSERM U1270, Paris, France

[5]Department of Biochemistry and Biophysics, University of California, San Francisco, CA 94143

[6]Chan Zuckerberg Biohub, San Francisco, CA94158, USA Chan Zuckerberg Biohub, San Francisco, CA 94158, USA

[7]Author for correspondence (email: thomas.theil@ed.ac.uk)

Running title: Inpp5e and direct/indirect neurogenesis

Key words: *Inpp5e*; *Tctn2*; primary cilia; neurogenesis; cortex

ABSTRACT

During the development of the cerebral cortex, neurons are generated directly from radial glial cells or indirectly via basal progenitors. The balance between these division modes determines the number and types of neurons formed in the cortex thereby affecting cortical functioning. Here, we investigate the role of primary cilia in controlling the decision between forming neurons directly or indirectly. We show that a mutation in the ciliary gene *Inpp5e* leads to a transient increase in direct neurogenesis and subsequently to an overproduction of layer V neurons in newborn mice. Loss of *Inpp5e* also affects ciliary structure coinciding with reduced Gli3 repressor levels. Genetically restoring Gli3 repressor rescues the decreased indirect neurogenesis in *Inpp5e* mutants. Overall, our analyses reveal how primary cilia determine neuronal subtype composition of the cortex by controlling direct versus indirect neurogenesis. These findings have implications for understanding cortical malformations in ciliopathies with *INPP5E* mutations.

INTRODUCTION

Building a functional cerebral cortex which confers humans with their unique cognitive capabilities requires controlling the proliferation of neural progenitor cells and the timing and modes of neurogenic cell divisions. Varying the timing and modes of neurogenesis affects neuronal numbers and subtype composition of the cortex (Florio & Huttner, 2014). In the developing murine cortex, radial glial cells (RGCs) represent the major neural stem cell type. Residing in the ventricular zone, they express Pax6 and undergo interkinetic nuclear migration dividing at the ventricular surface (Götz, Stoykova, & Gruss, 1998; Warren et al., 1999). Initially, RGCs go through rounds of symmetric proliferative divisions to produce two RGCs increasing the progenitor pool but switch to asymmetric divisions at the beginning of cortical neurogenesis. RGCs generate neurons in two ways, either directly or indirectly via the production of basal progenitors (BPs) that settle in the subventricular zone (SVZ) and express the Tbr2 transcription factor (Englund et al., 2005). In the mouse, the majority of BPs divide once to produce two neurons whereas the remainders undergo one additional round of symmetric proliferative division before differentiating into two neurons (Haubensak, Attardo, Denk, & Huttner, 2004; Miyata et al., 2004; Noctor, Martinez-Cerdeno, Ivic, & Kriegstein, 2004). In this way, BPs increase neuron output per radial glial cell and have therefore been implicated in the evolutionary expansion of the mammalian cerebral cortex (Martinez-Cerdeno, Noctor, & Kriegstein, 2006). Thus, the balance between direct and indirect neurogenesis is an important factor in generating appropriate neuron numbers and types.

The mechanisms that fine tune this balance and thereby adjust the numbers and types of neurons produced in the cortex have only recently been investigated. Mitotic spindle orientation (Postiglione et al., 2011) and endoplasmic reticulum (ER) stress (Gladwyn-Ng et al., 2018; Laguesse et al., 2015) are contributing factors to control the generation of basal progenitors. In addition, levels of Slit/Robo and Notch/Delta signaling were shown to be evolutionarily conserved factors that determine the predominant mode of neurogenesis (Cardenas et al., 2018). Moreover, feedback signals from postmitotic neurons control the fate of radial glial daughter cells involving the release of Neurotrophin-3 and Fgf9 (Parthasarathy, Srivatsa, Nityanandam, & Tarabykin, 2014; Seuntjens et al., 2009) as well as the activation of a Notch-dependent signaling pathway (W. Wang et al., 2016). These studies highlight the importance of cell-cell signaling in controlling the cell lineage of cortical progenitors (Silva, Peyre, & Nguyen, 2019) and emphasize the necessity of studying the cellular mechanisms by which these signals control the decision by RGCs to undergo direct or indirect neurogenesis.

Given the importance of cell-cell signaling, it is likely that the primary cilium, a signaling hub in embryogenesis in general and in neural development in particular (Valente, Rosti, Gibbs, & Gleeson, 2014), plays key roles in determining the balance between direct versus indirect neurogenesis. The cilium is a subcellular protrusion that predominately emanates from the apical surface of radial glial cells projecting into the ventricular lumen. The phenotypes of several mouse

lines mutant for ciliary genes underline the importance of the primary cilium in forebrain development but these mutants often suffer from severe patterning defects (Ashique et al., 2009; Besse et al., 2011; Willaredt et al., 2008) which make elucidating ciliary roles in determining the lineage of cortical progenitors difficult. To address how cilia control cortical progenitor development, we investigated corticogenesis in a mouse mutant for the ciliary gene *Inpp5e*.

INPP5E is mutated in Joubert syndrome (JS) (Bielas et al., 2009; Jacoby et al., 2009), a ciliopathy characterized by cerebellar defects in which a subset of patients also shows malformations of the cerebral cortex including heterotopias, polymicrogyria and agenesis of the corpus callosum (Valente et al., 2014). *Inpp5e* encodes Inositol polyphosphate 5 phosphatase E, an enzyme that is localized in the ciliary membrane and that hydrolyses the phosphatidylinositol polyphosphates $PI(4,5)P_2$ and $PI(3,4,5)P_3$ (Bielas et al., 2009; Jacoby et al., 2009). In this way, it controls the inositol phosphate composition of the ciliary membrane and thereby regulates the activity of several signaling pathways and cilia stability (Bielas et al., 2009; Chavez et al., 2015; Garcia-Gonzalo et al., 2015; Jacoby et al., 2009; Plotnikova et al., 2015). In contrast to *Inpp5e*'s extensively studied biochemical and cellular roles, little is known how these diverse functions are employed at the tissue level to control RGC lineage.

Here, we show that loss of *Inpp5e* function results in an increase in neuron formation at the expense of basal progenitor production in the E12.5 cortex and in an overproduction of Ctip2+ layer V neurons in newborn mutants. Moreover, RGC cilia show unusual membranous structures and/or abnormal numbers of microtubule doublets affecting the signaling capabilities of the cilium. The levels of Gli3 repressor (Gli3R), a critical regulator of cortical stem cell development (Hasenpusch-Theil et al., 2018; H. Wang, Ge, Uchida, Luu, & Ahn, 2011), is reduced and re-introducing Gli3R rescues the decreased formation of basal progenitors. Taken together, these findings implicate *Inpp5e* and the primary cilium in controlling the decision of RGCs to either undergo direct neurogenesis or to form basal progenitors, thereby governing the neuronal subtype composition of the cerebral cortex.

RESULTS

Inpp5e$^{\Delta/\Delta}$ embryos show mild telencephalic patterning defects

Controlling the balance between direct and indirect neurogenesis in the developing cerebral cortex is mediated by cell-cell signaling (Cardenas et al., 2018) and hence may involve the primary cilium. To investigate potential ciliary roles, we started characterizing cortical stem cell development in embryos mutant for the *Inpp5e* gene which has a prominent role in ciliary signaling and stability. Mutations in ciliary genes have previously been found to result in telencephalon patterning defects, most notably in a ventralisation of the dorsal telencephalon and/or in defects at the corticoseptal (CSB) and pallial/subpallial boundaries (PSPB) (Ashique et al., 2009; Besse et al., 2011; Willaredt et al., 2008). Therefore, we first considered the possibility that such early patterning defects may be present in *Inpp5e* mutant embryos and could affect cortical stem cell development. In situ hybridization and immunofluorescence analyses of E12.5 control and *Inpp5e*$^{\Delta/\Delta}$ embryos revealed no obvious effect on the expression of dorsal and ventral telencephalic markers at the corticoseptal boundary (Figure 1-figure supplement 1A-F). In contrast, the pallial/subpallial boundary was not well defined with a few scattered Pax6+ and *Dlx2* expressing cells on the wrong side of the boundary, i.e. in the subpallium and pallium, respectively (Figure 1-figure supplement 1G-L). Moreover, the hippocampal anlage appeared smaller and disorganized with low level and diffuse expression of cortical hem markers (Figure 1-figure supplement 2), consistent with known roles of Wnt/β-catenin and Bmp signaling in hippocampal development (Galceran, Miyashita-Lin, Devaney, Rubenstein, & Grosschedl, 2000; Lee, Tole, Grove, & McMahon, 2000). In contrast, progenitors in the neocortical ventricular zone of *Inpp5e* mutant mice expressed the progenitor markers *Emx1*, *Lhx2*, *Pax6* and *Ngn2,* though the levels of Pax6 protein expression appeared reduced in the medial neocortex suggestive of a steeper lateral to medial Pax6 expression gradient in mutant embryos. These expression patterns were maintained in E14.5 *Inpp5e*$^{\Delta/\Delta}$ embryos but revealed an area in the very caudal/dorsal telencephalon where the neocortex was folded (Figure 1-figure supplement 3). These folds became more prominent at more caudal levels and were also present in the hippocampal anlage. Taken together, these findings indicate that *Inpp5e* mutants have mild patterning defects affecting the integrity of the PSPB, hippocampal development and the caudal-most neocortex while the rostral neocortex shows no gross malformation or mispatterning and can therefore be analysed for effects of the *Inpp5e* mutation on direct and indirect neurogenesis.

Inpp5e controls direct vs indirect neurogenesis in the lateral neocortex

Based upon these findings, we started analyzing the proliferation and differentiation of radial glial cells in *Inpp5e*$^{\Delta/\Delta}$ embryos in the rostrolateral and rostromedial neocortex to avoid the regionalization defects described above. As a first step, we determined the proportion of radial glial cells, basal progenitors and neurons in these regions in E12.5 embryos. Double

immunofluorescence for PCNA which labels all progenitor cells (Hall et al., 1990) and the radial glial marker Pax6 did not reveal differences in the proportions of radial glial cells at both medial and lateral levels (Fig. 1A-D). In contrast, the proportion of Tbr2+ basal progenitors was reduced laterally but not medially (Fig. 1E-H). This decrease coincided with an increase in Tbr1+ neurons specifically in the lateral neocortex (Fig. 1I-L).

To determine whether these alterations are maintained at a later developmental stage, we repeated this investigation in E14.5 embryos. This analysis revealed no significant differences in the proportion of Pax6+ RGCs (Fig. 2A-D). Similarly, there was no alteration in the proportion of Tbr2+ basal progenitors in lateral neocortex, however, their proportion was reduced medially (Fig. 2E-H). To label cortical projection neurons, we used double immunofluorescence for Tbr1 and Ctip2 which allowed us to distinguish between Tbr1+Ctip2+ and Tbr1-Ctip2+ neurons. Quantifying these subpopulations showed no effect on the formation of Tbr1+ Ctip2+ neurons in *Inpp5e*$^{\Delta/\Delta}$ embryos. In contrast, the proportion of Tbr1- Ctip2+ neurons was reduced medially but increased in the lateral neocortex (Fig. 2I-N). Taken together with our E12.5 analyses, these findings show that in the lateral neocortex of *Inpp5e*$^{\Delta/\Delta}$ an increase in the proportion of Tbr1+ neurons at E12.5 is followed by an augmented fraction of Tbr1- Ctip2+ neurons at E14.5 whereas the proportion of basal progenitors recovered after an initial down-regulation.

To address the defective cellular processes underlying these neurogenesis defects in *Inpp5e* mutants, we first investigated programmed cell death and found few apoptotic cells in the control and mutant cortex (Figure 3-figure supplement 1). Next, we measured proliferation rates of cortical progenitors and performed double immunofluorescence for PCNA and pHH3 which labels mitotic radial glial cells located at the ventricular surface and dividing basal progenitors in abventricular positions (Figure 3-figure supplement 2). This analysis revealed no statistically significant differences in the E12.5 and E14.5 lateral neocortex of control and *Inpp5e*$^{\Delta/\Delta}$ embryos. The proportion of mitotic apical and basal progenitors, however, was reduced in the E12.5 medial neocortex (Figure 3-figure supplement 2). Interestingly, this decrease in the fraction of mitotic basal progenitors precedes the reduced proportion of basal progenitors in the E14.5 medial neocortex (Fig. 2E-H).

The cell cycle represents another key regulator of neuronal differentiation and a mutation in *Kif3a* affects ciliogenesis and the cell cycle in the developing neocortex (Wilson, Wilson, Wang, Wang, & McConnell, 2012). To investigate the possibility of altered cell cycle kinetics, we used a BrdU/IdU double labelling strategy (Martynoga, Morrison, Price, & Mason, 2005; Nowakowski, Lewin, & Miller, 1989) to determine S phase length and total cell cycle length in radial glial cells and found no statistically significant changes in these parameters (Figure 3-figure supplement 3).

Finally, the increased neuron production could also be explained by an increase in direct neurogenesis at the expense of basal progenitor cell formation. To test this possibility, we gave BrdU to E11.5 pregnant mice 24h before dissecting the embryos. We then used BrdU immunostaining in conjunction with Tbr1 and Tbr2 to identify the neurons and basal progenitors formed in the lateral neocortex within the 24h time period. This analysis showed that the proportion of Tbr1+ neurons

compared to the total number of BrdU+ cells increased while the Tbr2+ proportion decreased in *Inpp5e* mutants (Fig. 3). Since the cell cycle of basal progenitors is longer than 24h (Arai et al., 2011), the 24h interval used in our cell cycle exit experiment was too short for newly formed basal progenitors to undergo one additional round of the cell cycle and as the BrdU label would have been diluted with a further round of division, this analysis supports our hypothesis that direct neurogenesis became more prevalent in *Inpp5e*$^{\Delta/\Delta}$ radial glial cells.

Cortical malformations in *Inpp5e*$^{\Delta/\Delta}$ embryos

Next, we investigated the consequences of this increase in direct neurogenesis on cortical size and layer formation. Since *Inpp5e*$^{\Delta/\Delta}$ newborn pups die perinatally (Bielas et al., 2009), we focused our analysis on E18.5 embryos. The mutant lacked obvious olfactory bulbs, as revealed by whole mounts of control and mutant brains (Figure 4-figure supplement 1). To gain insights into the overall histology of the mutant forebrain, we stained coronal sections with DAPI. This analysis showed that most of the mutant cortex was thinner except for the rostrolateral level (Figure 4-figure supplement 2). In addition, the hippocampus was malformed with a smaller dentate gyrus. Investigating the expression of markers characteristic of the entire hippocampus (*Nrp2*; (Galceran et al., 2000)), the CA1 field (Scip1; (Frantz, Bohner, Akers, & McConnell, 1994)) and the dentate gyrus (Prox1; (Oliver et al., 1993)) showed that these hippocampal structures were present but were severely reduced in size and disorganized in *Inpp5e*$^{\Delta/\Delta}$ embryos (Figure 4-figure supplement 3). In addition, the corpus callosum, the major axon tract connecting the two cerebral hemispheres, was smaller. We confirmed this effect by staining callosal axons and surrounding glial cells that guide these axons to the contralateral hemisphere with L1 and GFAP, respectively (Figure 4-figure supplement 4).

After characterizing the gross morphology of the *Inpp5e*$^{\Delta/\Delta}$ cortex, we next investigated whether the increased neuron formation in E12.5 mutant embryos led to changes in the neuronal subtype composition of the E18.5 cortex. To this end, we used immunofluorescence labelling for Tbr1 and Ctip2 to analyse the formation of layer VI and V neurons, respectively, whereas Satb2 served as a layer II-IV marker (Fig. 4). Inspecting these immunostainings at low magnification showed that Tbr1+, Ctip2+ and Satb2+ neurons occupied their correct relative laminar positions in *Inpp5e* mutants (Fig. 4A-F) except for neuronal heterotopias which were present in all mutant brains, though their number and position varied (Fig. 4D). These immunostainings also revealed a medial shift in the position of the rhinal fissure, a sulcus that is conserved across mammalian species and separates neocortex from the paleocortical piriform cortex (Ariens-Kapers, Huber, & Crosby, 1936). This shift was more marked caudally and suggests a dramatic expansion of the *Inpp5e* mutant piriform cortex at the expense of neocortex at caudal most levels (Fig. 4D-F). Using the Tbr1/Ctip2 and Satb2 stainings, we determined the proportions of deep and superficial layer neurons, respectively. Because of the expanded piriform cortex in *Inpp5e* mutants, we limited this

investigation to the unaffected rostral neocortex. In the rostrolateral neocortex, we found the proportion of Tbr1+ neurons to be reduced (Fig. 4G, H, M). This reduction coincided with an increased proportion of Ctip2+ layer V neurons (Fig. 4I, J, N) while the Satb2 population was unchanged (Fig. 4K, L, O). In contrast, the rostromedial neocortex did not show any differences (Fig. 4P-X). Thus, the increase in direct neurogenesis in the lateral neocortex during earlier development concurs with a change in the proportions of E18.5 Tbr1+ and Ctip2+ deep layer neurons.

A mutation in the ciliary gene *Tctn2* leads to increased telencephalic neurogenesis

To start to unravel the mechanisms by which *Inpp5e* controls cortical stem cell development, we first analysed whether the increased early neurogenesis is restricted to *Inpp5e*$^{\Delta/\Delta}$ mutants or is observed in another mutant affecting cilia. To this end, we focused on the *TECTONIC* 2 (*TCTN2*) gene which is crucial for ciliary transition zone architecture (Shi et al., 2017) and which, like *INPP5E*, is mutated in Joubert Syndrome (Garcia-Gonzalo et al., 2011). Interestingly, E12.5 *Tctn2*$^{\Delta/\Delta}$ mutant embryos (Reiter & Skarnes, 2006) also showed an increased proportion of Tbr1+ projection neurons and a concomitant decrease in Tbr2+ basal progenitors in the dorsolateral telencephalon (Fig. 5). Due to embryonic lethality, however, we were not able to investigate the formation of cortical neurons at later stages.

Ciliary defects in the forebrain of E12.5 *Inpp5e*$^{\Delta/\Delta}$ embryos

Our findings in the *Inpp5e* and *Tctn2* mutants suggested a role for cilia in cortical progenitor cells to control early neurogenesis. Therefore, we examined the presence and the structure of primary cilia in the developing forebrain of *Inpp5e*$^{\Delta/\Delta}$ embryos by immunofluorescence and electron microscopy. We first analyzed the presence of the small GTPase Arl13b, enriched in ciliary membranes, and of γ-Tubulin (γTub), a component of basal bodies (Caspary, Larkins, & Anderson, 2007). We found no major difference in the number or the apical localization of cilia in control and *Inpp5e*$^{\Delta/\Delta}$ neuroepithelial cells in the E12.5 telencephalon (Fig. 6A,B) or diencephalon (data not shown).

To gain insights into the fine structure of these primary cilia we performed electron microscopy analyses. Scanning electron microscopy (SEM) provided an observation of the cilia protruding into the telencephalic ventricles. In control embryos, almost all radial glial cells had a single, ~1 μm long primary cilium (Fig. 6C), as previously described (Besse et al., 2011). Some *Inpp5e*$^{\Delta/\Delta}$ mutant cells also displayed an apparently normal cilium (Fig. 6D, E), whereas other cells harbored abnormal cilia, either with a lateral blob (arrowhead in Fig. 6D, E) or as a short and bloated cilium-like protrusion (arrows in Fig. 6D,E).

Transmission electron microscopy (TEM) confirmed the presence of abnormal cilia in *Inpp5e*$^{\Delta/\Delta}$ embryos. Cilia were recognized by basal bodies anchored to the apical membrane in both control and *Inpp5e*$^{\Delta/\Delta}$ radial glial cells (Fig. 6F-L, N, Q). However, in *Inpp5e*$^{\Delta/\Delta}$ cells, some cilia lacked

the axoneme and showed unusual membranous structures that resemble budding vesicles emerging from the lateral surface of the cilium (Fig. 6G, K), internal vesicles (arrows in Fig. 6I, K, L), or undulating peripheral membranes (Fig. 6I), indicating an *Inpp5e*-dependent defect in ciliary membrane morphology. Transverse sections revealed the presence of cilia with apparently normal 9+0 axonemes, as well as cilia containing abnormal numbers of microtubule doublets in *Inpp5e*$^{\Delta/\Delta}$ embryos (Fig. 6O, P). To quantify these ciliary defects, we counted the number of normal versus abnormal cilia on TEM images obtained from control and *Inpp5e*$^{\Delta/\Delta}$ embryos, and found an increase in abnormal cilia in *Inpp5e*$^{\Delta/\Delta}$ compared to control embryos (Fig. 6R). Taken together, a significant number of abnormal primary cilia were found at the apical end of E12.5 radial glial cells in the forebrain of *Inpp5e*$^{\Delta/\Delta}$ embryos. These abnormalities are consistent with a role of *Inpp5e* in maintaining cilia stability (Jacoby et al., 2009).

Restoring Gli3 repressor ratio rescues cortical malformations in *Inpp5e*$^{\Delta/\Delta}$ embryos

Primary cilia play a crucial role in Shh signaling by controlling the proteolytic cleavage of full length Gli3 (Gli3FL) into the Gli3 repressor form (Gli3R) in the absence of Shh and by converting Gli3FL into the transcriptional activator Gli3A in the presence of Shh. Moreover, the dorsal telencephalon predominately forms Gli3R (Fotaki, Yu, Zaki, Mason, & Price, 2006) and mice that can only produce Gli3R have no obvious defect in cortical development (Besse et al., 2011; Böse, Grotewold, & Rüther, 2002). In addition, we recently showed that Gli3 has a prominent role in radial glial cells controlling the switch from symmetric proliferative to asymmetric neurogenic cell division (Hasenpusch-Theil et al., 2018). Therefore, we hypothesized that alterations in Gli3 processing caused by abnormal cilia function underlies the increased direct neurogenesis and the cortical malformations in *Inpp5e*$^{\Delta/\Delta}$ embryos. In situ hybridization showed that *Gli3* mRNA expression might be slightly reduced but the overall expression pattern in the telencephalon remains unaffected (Figure 7-figure supplement 1). We next investigated the formation of Gli3FL and Gli3R in the E12.5 dorsal telencephalon of *Inpp5e*$^{\Delta/\Delta}$ embryos using Western blots. This analysis revealed no change in the levels of Gli3FL but a significant decrease inGli3R which resulted in a reduced Gli3R to Gli3FL ratio in the mutant (Fig. 7A-D) suggesting that the *Inpp5e* mutation affects Gli3 processing.

The next set of experiments aimed to clarify a role for the reduced Gli3 processing. To this end, we restored Gli3R levels by crossing *Inpp5e* mutants with *Gli3*$^{\Delta 699/+}$ mice that can only produce Gli3R in a cilia-independent manner (Besse et al., 2011; Böse et al., 2002). Overall inspection of *Inpp5e*$^{\Delta/\Delta}$;*Gli3*$^{\Delta 699/+}$ embryos revealed restored eye formation whereas *Inpp5e*$^{\Delta/\Delta}$ embryos either completely lacked eyes or showed microphthalmia (Jacoby et al., 2009) (Figure 7-figure supplement 2). Moreover, the overall morphology of the telencephalon is much improved in *Inpp5e*$^{\Delta/\Delta}$;*Gli3*$^{\Delta 699/+}$ embryos as compared to *Inpp5e*$^{\Delta/\Delta}$ embryos. In E18.5 *Inpp5e*$^{\Delta/\Delta}$ *Gli3*$^{\Delta 699/+}$ mutants, the corpus callosum has a thickness indistinguishable from that of control embryos (Figure 7-figure supplement

3). In E12.5 and E14.5 *Inpp5e*$^{\Delta/\Delta}$;*Gli3*$^{\Delta 699/+}$ embryos, the neocortex lacks the undulations of the VZ present in *Inpp5e*$^{\Delta/\Delta}$ embryos (data not shown) and the morphology of the hippocampal anlage is more akin to that in wild-type embryos but it is still smaller and less bulged (Fig. 7E, G, I).

We also determined the proportions of basal progenitors and Tbr1+ neurons at E12.5 which were decreased and increased, respectively, in the lateral neocortex of *Inpp5e*$^{\Delta/\Delta}$ embryos. While these changes were still present in *Inpp5e*$^{\Delta/\Delta}$ littermate embryos, there was no statistically significant difference between control and *Inpp5e*$^{\Delta/\Delta}$;*Gli3*$^{\Delta 699/+}$ embryos (Fig. 7E-L). This finding indicates that the neurogenesis phenotype of E12.5 *Inpp5e*$^{\Delta/\Delta}$ mutants is rescued by a single copy of the Gli3$^{\Delta 699}$ allele. We next investigated the formation of basal progenitors and of cortical projection neurons in E14.5 *Inpp5e*$^{\Delta/\Delta}$;*Gli3*$^{\Delta 699/+}$ embryos. The proportion of Tbr1+Ctip2+ neurons was not affected in the medial neocortex of E14.5 *Inpp5e*$^{\Delta/\Delta}$;*Gli3*$^{\Delta 699/+}$ embryos. In contrast, the proportion of Tbr1-Ctip2+ neurons was reduced as in *Inpp5e*$^{\Delta/\Delta}$ mutants (Fig. 8A, C, E, I, J). Similarly, the proportions of basal progenitors in the medial *Inpp5e*$^{\Delta/\Delta}$ *Gli3*$^{\Delta 699/+}$ neocortex was slightly improved compared to *Inpp5e*$^{\Delta/\Delta}$ embryos but significantly smaller than in control embryos (Fig. 8B, D, F, K). As re-introducing a single Gli3$^{\Delta 699}$ allele does not completely rescue the *Inpp5e*$^{\Delta/\Delta}$ neurogenesis phenotype, we generated *Inpp5e*$^{\Delta/\Delta}$ embryos homozygous for the *Gli3*$^{\Delta 699}$ allele. Interestingly, the morphology of the dorsal telencephalon including the hippocampal formation was indistinguishable between control and *Inpp5e*$^{\Delta/\Delta}$;*Gli3*$^{\Delta 699/\Delta 699}$ embryos (Fig. 8A, B, G, H) and the formation of Tbr1-Ctip2+ neurons and Tbr2+ basal progenitors were not affected (Fig. 8G, H, J, K). Taken together, these findings indicate that re-introducing a single copy of the *Gli3R* allele into the *Inpp5e* mutant background leads to a partial rescue of cortical neurogenesis in *Inpp5e*$^{\Delta/\Delta}$ embryos whereas two copies are required for a full rescue.

DISCUSSION

Generating a functional cerebral cortex requires a finely tuned balance between direct and indirect neurogenesis to form subtypes of cortical projection neurons in appropriate numbers. Here, we show that the ciliary mouse mutants *Inpp5e* and *Tctn2* present with a transient increase in neurons forming directly from radial glia progenitors in the lateral neocortex at the expense of basal progenitor formation. This increase in neurogenesis results in augmented formation of Ctip2+ layer V neurons in the *Inpp5e* mutant cortex. Our studies also revealed that the *Inpp5e* mutation interfered with the stability of the RGC primary cilium and its signaling functions, leading to a reduction in the Gli3R levels. Since re-introducing Gli3R in an *Inpp5e* mutant background restored the decreased formation of normal proportions of basal progenitors and neurons, our findings implicate a novel role for primary cilia in controlling the signaling events that direct the decision of RGCs to undergo either direct or indirect neurogenesis.

Primary cilia affect the decision between direct and indirect neurogenesis

Radial glial cells in the developing mouse neocortex have the potential to undergo symmetric proliferative or asymmetric cell divisions with the latter division mode producing neurons in a direct manner or indirectly via basal progenitors. Balancing out these division modes is important not only to determine final neuronal output and cortical size but also the types of cortical projection neurons and, hence, subtype composition of the adult neocortex. In the E12.5 *Inpp5e* and *Tctn2* mouse mutants, we identified an increased formation of neurons in the lateral neocortex. Based on our cell cycle exit experiment additional neurons are formed from RGCs at the expense of basal progenitors. Given the cell cycle length of basal progenitors of >24 hours (Arai et al., 2011), it is unlikely that new born basal progenitors would have undergone an additional round of cell division to produce two neurons within the time frame of this experiment. Such an extra division would also have diluted the BrdU label. We therefore conclude that the *Inpp5e* mutation caused RGCs to preferentially produce neurons directly. Moreover, neurogenesis defects only became obvious at E14.5 in the medial neocortex. This delay might reflect the neurogenic gradient in the neocortex or might be related to specific gene expression changes such as reduced Pax6 expression in medial neocortical progenitors.

Interestingly, the increase in direct neurogenesis led to an increased proportion of Ctip2+ deep layer V neurons in the E18.5 neocortex but did not coincide with a reduced proportion of upper layer neurons. This effect could be explained in several mutually non-exclusive ways. First, neurons born at E12.5 initially express both Ctip2 and Tbr1 (Fig. 7) and later down-regulate Ctip2. *Inpp5e* could therefore affect the signaling that controls this downregulation. Secondly, the proportions of basal progenitors and neurons were normalized in E14.5 mutants. Since basal progenitors are a main source of upper layer neurons (Arnold et al., 2008; Vasistha et al., 2015), this normalization would account for the sufficient numbers of Satb2+ upper layer neurons. Newly formed projection neurons signal back to RGCs via Jag1, Fgf9 and Neurotrophin 3 (Parthasarathy et al., 2014;

Seuntjens et al., 2009; W. Wang et al., 2016) to control the sequential production of deep and upper layer neurons and of glia (Silva et al., 2019). *Inpp5e* might affect these signals by controlling cilia stability and/or levels of $PI(3,4,5)P_3$ (Bielas et al., 2009; Jacoby et al., 2009) that acts as a second messenger in receptor tyrosine kinase signaling. Regardless of the exact mechanism, our findings suggest a novel, spatially and temporally restricted role for *Inpp5e* in controlling the decision between direct and indirect neurogenesis. This function differs from those described for other cilia mutants. Conditional inactivation of *Ift88* and *Kif3a* leads to a larger cortex (Foerster et al., 2017; Wilson et al., 2012) with a modest increase in BP production in the absence of a delay in neurogenesis (Foerster et al., 2017) while *Rpgrip1l* mutants have reduced numbers of both basal progenitors and neurons (Postel, Karam, Pezeron, Schneider-Maunoury, & Clement, 2019). These findings highlight the multiple and varied roles cilia play in cortical development.

Inpp5e controls direct/indirect neurogenesis through Gli3 processing

Our study also shed lights into the mechanisms by which *Inpp5e* controls the decision between direct and indirect neurogenesis. Most notably, the Gli3R level and Gli3R/Gli3FL ratio are decreased in $Inpp5e^{\Delta/\Delta}$ embryos. While the *Inpp5e* mutation does not lead to an up-regulation of Shh signaling in the dorsal telencephalon (Magnani et al., 2015), re-introducing a single or two copies of Gli3R in an *Inpp5e* mutant background partially and fully restores the neurogenesis defects, respectively. This rescue indicates that reduced levels of Gli3R rather than the reduction in the Gli3R/Gli3FL ratio are responsible for the prevalence of direct neurogenesis in $Inpp5e^{\Delta/\Delta}$ embryos. This idea is consistent with the findings that (i) $Gli3^{\Delta 699/\Delta 699}$ embryos that cannot produce Gli3FL and Gli3A show no obvious phenotype in cortical development (Besse et al., 2011; Böse et al., 2002), (ii) dorsal telencephalic patterning defects in $Gli3^{Xt/Xt}$ mutants are not rescued in $Shh^{-/-}/Gli3^{XtXt}$ double mutants (Rallu et al., 2002; Rash & Grove, 2007), (iii) Shh promotes the generation of olfactory bulb interneurons and cortical oligodendrocytes and neurogenesis in the subventricular zone by reducing Gli3R rather than by promoting Gli activator function (Petrova, Garcia, & Joyner, 2013; H. Wang, Kane, Lee, & Ahn, 2014; Zhang et al., 2020). In addition, there is also a dramatic rescue of eye development and the rescue also extends to other malformations of the $Inpp5e^{\Delta/\Delta}$ forebrain, including the corpus callosum, the hippocampus and the expansion of the piriform cortex, structures that are also affected in *Gli3* null and hypomorphic mutants (Amaniti et al., 2015; Johnson, 1967; Magnani et al., 2014; Theil, Alvarez-Bolado, Walter, & Rüther, 1999; Wiegering, Petzsch, Kohrer, Ruther, & Gerhardt, 2019). Taken together, these findings support the idea that *Inpp5e* and the primary cilium control key processes in cortical development by regulating the formation of Gli3R.

Our analyses support several mutually non-exclusive mechanisms how the *Inpp5e* mutation impacts on Gli3 processing. First, our electron microscopy study revealed severe structural abnormalities in large proportions of cilia. The Inpp5e phosphatase hydrolyses $PI(3,4,5)P_3$, which is essential for the effective activation of the serine threonine kinase Akt (Kisseleva, Cao, & Majerus, 2002; Plotnikova et al., 2015). Following $PI(3,4,5)P_3$ binding, Akt translocates to the membrane and

becomes phosphorylated at T308 by phosphoinositide dependent kinase-1 (Pdk1) and at S473 by mammalian target of rapamycin complex (mTORC2) (Yu & Cui, 2016). Consistent with the loss of *Inpp5e* function and a resulting increase in $PI(3,4,5)P_3$, western blot analysis revealed elevated $pAkt^{S473}$ levels (data not shown). Increased phosphorylation at this site has been implicated in inhibiting cilia assembly and promoting cilia disassembly (Mao et al., 2019) and could hence explain the structural defects of RGC *Inpp5e*$^{\Delta/\Delta}$ cilia. Secondly, *Inpp5e* could control Gli3 processing through its effect on the transition zone (TZ). It is required for TZ molecular organisation (Dyson et al., 2017) and its substrate PI(4,5)P2 plays a role in TZ maturation in Drosophila (Gupta, Fabian, & Brill, 2018). This model is further supported by our finding that a mouse mutant for the TZ protein Tctn2 phenocopies the *Inpp5e*$^{\Delta/\Delta}$ neurogenesis defect. In turn, several mouse mutants defective for TZ proteins are required for Inpp5e localization to cilia and show microphthalmia (Garcia-Gonzalo et al., 2011; Garcia-Gonzalo et al., 2015; Sang et al., 2011; Yee et al., 2015). Tctn proteins are also required for Gli3 processing (Garcia-Gonzalo et al., 2011; Sang et al., 2011; Thomas et al., 2012; C. Wang, Li, Meng, & Wang, 2017) and the TZ protein Rpgrip1l controls the activity of the proteasome at the basal body responsible for proteolytic cleavage of Gli3 (Gerhardt et al., 2015). Taken together, these findings indicate that *Inpp5e* mutation might affect the ability of RGCs to switch to indirect neurogenesis through defects in cilia stability and/or the integrity of the ciliary transition zone (Fig. 9).

Implications for Joubert Syndrome

In humans, hypomorphic *INPP5E* mutations contribute to Joubert Syndrome (JS), a ciliopathy characterized by cerebellar malformations and concomitant ataxia and breathing abnormalities. In addition, a subset of JS patients exhibit cortical abnormalities including polymicrogyria, neuronal heterotopias and agenesis of the corpus callosum (Poretti, Huisman, Scheer, & Boltshauser, 2011). Strikingly, the *Inpp5e* mouse mutant also shows several of these abnormalities. In the caudal telencephalon, the otherwise lissencephalic cortex formed folds reminiscent of the polymicrogyria in JS patients. In addition, the mutant formed leptomeningeal heterotopias with 100% penetrance, but their number and location varied. Mutations in ciliary genes were previously associated with heterotopia formation in humans and mice (Magnani et al., 2015; Uzquiano et al., 2019). Mice carrying mutations in the *Eml1* gene encoding a microtubule-associated protein show subcortical heterotopias due to a mispositioning of radial glial cells and impaired primary cilia formation (Uzquiano et al., 2019). Finally, the corpus callosum is thinner but callosal axons project to the contralateral cerebral hemisphere in *Inpp5e* mutants. This phenotype is milder compared to that of other mouse mutants with altered cilia that show complete agenesis of the corpus callosum with callosal axons forming Probst bundles (Benadiba et al., 2012; Laclef et al., 2015; Putoux et al., 2019). Unlike these other ciliary mutants, the corticoseptal boundary which plays a crucial role in positioning guidepost cells that control midline crossing of callosal axons (Magnani et al., 2014) is not obviously affected in *Inpp5e*$^{\Delta/\Delta}$ embryos. Instead, the thinner corpus callosum is

likely to be the result of reduced size of the caudal neocortex. Despite these differences, however, re-introducing Gli3R into the cilia mutant background restores callosal development in both groups of mutants suggesting that cilia control two independent steps in corpus callosum formation by regulating Gli3 processing. Thus, the *Inpp5e*$^{\Delta/\Delta}$ mutant recapitulates cortical abnormalities in JS patients and starts to help unravelling the pathomechanisms underlying these defects.

Key Resources Table				
Reagent type (species) or resource	**Designation**	**Source or reference**	**Identifiers**	**Additional information**
genetic reagent (*Mus musculus*)	Inpp5e^{delta} (Inpp5e$^{tm1.2Sch}$)	PMID: 19668215	MGI:4360187	
genetic reagent (*Mus musculus*)	Gli3^{delta699} (Gli3^{tm1Urt})	PMID: 11978771	MGI:2182576	
genetic reagent (*Mus musculus*)	Tctn2^{delta} (Tctn2$^{tm1.1Reit}$)	PMID: 21725307	MGI:5292130	
antibody	anti-Arl13b (clone N295B/66) (Mouse monoclonal)	UC Davis/NIH NeuroMab Facility	Cat# 75-287 RRID:AB_11000053	IF (1:1500)
antibody	anti-BrdU (Rat monoclonal)	Abcam	Cat# ab6326 RRID:AB_305426	IF (1:50)
antibody	anti-BrdU/IdU (B44) (Mouse monoclonal)	BD Biosciences	Cat# 347580 RRID:AB_2313824	IF (1:500)
antibody	cleaved-Caspase3 (Asp175) (5A1E) (Rabbit polyclonal)	Cell Signaling Technology	Cat# 9664 RRID:AB_2070042	IF (1:100)
antibody	anti-Ctip2 (Rat monoclonal)	Abcam	Cat# ab18465 RRID:AB_2064130	IF (1:1000)

antibody	anti-GFAP (Rabbit polyclonal)	Agilent	Cat# Z0334 RRID:AB_10013382	IF (1:1000)
antibody	anti-L1, clone 324 (Rat monoclonal)	Millipore	Cat# MAB5272 RRID:AB_2133200	IF (1:1000)
antibody	anti-Pax6 (Rabbit polyclonal)	Biolegend	Cat# 901301 RRID:AB_2565003	IF (1:400)
antibody	anti-PCNA (PC10) (Mouse monoclonal)	Abcam	Cat# ab29 RRID:AB_303394	IF (1:500)
antibody	anti-Prox1 (Rabbit polyclonal)	Reliatech	Cat# 102-PA32 RRID:AB_10013821	IHC (1:1000)
A9ntibody	anti-pHH3 (Rabbit polyclonal)	Millipore	Cat# 06-570 RRID:AB_310177	IF (1:100)
antibody	anti-Satb2 (Mouse monoclonal)	Abcam	Cat# ab51502 RRID:AB_882455	IF (1:200)
antibody	anti-Tbr1 (Rabbit polyclonal)	Abcam	Cat# ab31940 RRID:AB_2200219	IF (1:400)
antibody	anti-Tbr2 (Rabbit polyclonal)	Abcam	Cat# ab23345 RRID:AB_778267	IF (1:1000)

antibody	anti–γTUB, (Rabbit polyclonal)	Sigma Aldrich	Cat# SAB4503045 RRID:AB_10747615	IF (1:100)
antibody	anti-mouse Cy2 secondary (Donkey polyclonal)	Jackson ImmunoResearch Labs	Cat# 715-225-151 RRID:AB_2340827	IF (1:100)
antibody	anti-rabbit Cy3 secondary (Donkey polyclonal)	Jackson ImmunoResearch Labs	Cat# 711-165-152	IF (1:100)
antibody	anti-rat Cy3 secondary (Goat polyclonal	Jackson ImmunoResearch Labs	Cat# 711-165-152 RRID:AB_2307443	IF (1:100)
antibody	Anti-rabbit Alexa Fluor 488 secondary (Goat polyclonal	Molecular Probes (now: Invitrogen)	Cat# A-11008 RRID:AB_143165	IF (1:200)
antibody	anti-rat Alexa Fluor 647 secondary (Goat polyclonal)	Molecular Probes (now: Invitrogen)	Cat# A-21247 RRID:AB_141778	IF (1:200)
antibody	Biotinylated swine anti-rabbit IgG	Dako	Cat# E0431	IF (1:400)
antibody	Streptavidin, Alexa Fluor 488 conjugate antibody	Molecular Probes (now: Invitrogen)	Cat# S32354 RRID:AB_2315383	IF (1:100)

antibody	Streptavidin, Alexa Fluor® 568 conjugate antibody	Thermo Fisher Scientific	Cat# S-11226 RRID:AB_2315774	IF (1:100)
antibody	biotinylated goat anti-rabbit IgG	Dako (now: Agilent)	Cat# E0432 RRID:AB_2313609	IF (1:400)
antibody	anti-h/m Gli3 (Goat polyclonal)	R&D Systems	Cat# AF3690 RRID:AB_2232499	WB (1:500)
antibody	anti-β-Actin (clone AC-15) (Mouse monoclonal)	Abcam	Cat# ab6276 RRID:AB_2223210	WB (1:15,000)
antibody	IRDye 680RD Donkey anti-Goat IgG	LI-COR Biosciences	Cat# 926-68074 RRID:AB_10956736	WB (1:15,000)
antibody	IRDye 800CW Donkey anti-Mouse IgG	LI-COR Biosciences	Cat# 925-32212 RRID AB_2716622	WB (1:15,000)
commercial assay or kit	VECTASTAIN Elite ABC-Peroxidase Kit	Vector Laboratories	Cat# PK-6100 RRID:AB_2336819	
chemical compound, drug	IdU 5-Iodo-2′-deoxyuridine	Sigma Aldrich	Cat# I7125	(10mg/ml)
chemical compound, drug	BrdU 5-Bromo-2′-deoxyuridine	Sigma Aldrich	Cat# B5002	(10mg/ml)
software, algorithm	Fiji	PMID: 22743772?	PRID:SCR_002285	http://imagej.net/Fiji

software, algorithm	Image Studio Lite	Li-Cor	4.0	
software, algorithm	GraphPad Prism	GraphPad Software	8.4.2 (679)	
software, algorithm	Adobe Photoshop	Adobe Inc.	12.1	
other	DAPI (4',6-Diamidino-2-Phenylindole, Dihydrochloride)	Thermo Fisher Scientific	Cat# D1306 RRID:AB_2629482	IF (1:2000)

MATERIAL & METHODS

Mice

All experimental work was carried out in accordance with the UK Animals (Scientific Procedures) Act 1986 and UK Home Office guidelines. All protocols were reviewed and approved by the named veterinary surgeons of the College of Medicine and Veterinary Medicine, the University of Edinburgh, prior to the commencement of experimental work. *Inpp5e*$^{\Delta}$ (*Inpp5*e^{delta}), *Gli3*$^{\Delta 699}$ (*Gli3*^{delta699}) and *Tctn2*$^{\Delta}$ (*Tctn2*$^{tm1.1Reit}$) mouse lines have been described previously (Böse et al., 2002; Garcia-Gonzalo et al., 2011; Jacoby et al., 2009). *Inpp5e*$^{\Delta/+}$ mice were interbred to generate *Inpp5e*$^{\Delta/\Delta}$ embryos; exencephalic *Inpp5e*$^{\Delta/\Delta}$ embryos which made up ca. 25% of homozygous mutant embryos were excluded from the analyses. Wild-type and *Inpp5e*$^{\Delta/+}$ litter mate embryos served as controls. *Inpp5e*$^{\Delta/\Delta}$;*Gli3*$^{\Delta 699/+}$ and *Inpp5e*$^{\Delta/\Delta}$;*Gli3*$^{\Delta 699/\Delta 699}$ embryos were obtained from inter-crosses of *Inpp5e*$^{\Delta/+}$;*Gli3*$^{\Delta 699/+}$ mice using wild-type, *Inpp5e*$^{\Delta/+}$ and *Gli3*$^{\Delta 699/+}$ embryos as controls. Embryonic (E) day 0.5 was assumed to start at midday of the day of vaginal plug discovery. Transgenic animals and embryos from both sexes were genotyped as described (Böse et al., 2002; Jacoby et al., 2009). For each marker and each stage, 3-8 embryos were analysed.

For measuring cell cycle lengths, pregnant females were intraperitoneally injected with a single dose of IdU (Sigma-Aldrich) (10mg/ml) at E12.5, followed by an injection of BrdU Sigma-Aldrich) (10mg/ml) 90 min later. Embryos were harvested 30 min after the second injection. For cell cycle exit analyses, BrdU was injected peritoneally into E11.5 pregnant females and embryos were harvested 24 hrs later.

Immunohistochemistry and in situ hybridisation

For immunohistochemistry, embryos were fixed overnight in 4% paraformaldehyde, incubated in 30% sucrose at +4°C for 24h, embedded in 30% sucrose/OCT mixture (1:1) and frozen on dry ice. Immunofluorescence staining was performed on 12 to 14 μm cryostat sections as described previously (Theil, 2005) with antibodies against Arl13b (mouse) (Neuromab 75-287; 1:1500), rat anti-BrdU (1:50, Abcam #ab6326), mouse anti-BrdU/IdU (B44) (1:50, BD Biosciences #347580), rabbit anti-Cleaved Caspase 3 (1:100, Cell Signaling Technology, #9664), rat anti-Ctip2 (1:1000, Abcam #ab18465), rabbit anti-GFAP (1:1000, Agilent/Dako #Z 0334), rat anti-L1, clone 324 (1:1000, Millipore #MAB5272), rabbit anti-Pax6 (1:400, Biolegend #901301), mouse anti-PCNA (1:500, Abcam #ab29), rabbit anti-Prox1 (1:1000, RELIA*Tech* #102-PA32). rabbit anti-pHH3 (1:100, Millipore #06-570), mouse anti-Satb2 (1:200, Abcam #ab51502), rabbit anti-Tbr1 (1:400, Abcam #ab31940), rabbit anti-Tbr2 (1:1000, Abcam #ab23345) and rabbit anti-γTUB (Sigma-Aldrich SAB4503045; 1:100). Primary antibodies for immunohistochemistry were detected with Alexa- or Cy2/3-conjugated fluorescent secondary antibodies. The Cleaved Caspase 3 and Tbr1 signals were amplified using biotinylated secondary IgG antibody (swine anti-rabbit IgG) (1:400, Dako) followed by Alexa Fluor 488 (1:100, Invitrogen) or 568 Streptavidin (1:100, Thermo Fisher Scientific). For counter staining DAPI (1:2000, Thermo Fisher Scientific) was used. Prox1 protein was detected non-fluorescently using biotinylated goat anti-rabbit IgG (1: 400,Agilent (Dako)) followed by avidin-HRP and DAB detection using Vectastain Elite ABC peroxidase kit (Vector laboratories) as described previously (Magnani et al., 2010).

In situ hybridisation on 12μm serial paraffin sections were performed as described previously (Theil, 2005) using antisense RNA probes for *Axin2* (Lustig et al., 2002), *Bmp4* (Jones, Lyons, & Hogan, 1991), *Dbx1* (Yun, Potter, & Rubenstein, 2001), *Dlx2* (Bulfone et al., 1993), *Emx1* (Simeone et al., 1992), *Gli3* (Hui, Slusarski, Platt, Holmgren, & Joyner, 1994), *Lhx2* (Liem, Tremml, & Jessell, 1997), *Msx1 (Hill et al., 1989)*, *Ngn2* (Gradwohl, Fode, & Guillemot, 1996), *Nrp2* (Galceran et al., 2000), *Pax6* (Walther & Gruss, 1991), *Scip1* (Frantz et al., 1994), *Wnt2b* (Grove, Tole, Limon, Yip, & Ragsdale, 1998).

Western blot

Protein was extracted from the dorsal telencephalon of E12.5 wild-type and *Inpp5e*$^{\Delta/\Delta}$ embryos (n=4 samples per genotype) as described previously (Magnani et al., 2010). 10μg protein lysates were subjected to gel electrophoresis on a 3-8% NuPAGE® Tris-Acetate gel (Life Technologies), and protein was transferred to a Immobilon-FL membrane (Millipore), which was incubated with goat anti-h/m Gli3 (1:500, R&D Systems #AF3690) and mouse anti-β-Actin antibody (1:15000, Abcam #ab6276). After incubating with donkey anti-goat IgG IRDye680RD (1:15000, LI-COR Biosciences) and donkey anti-mouse IgG IRDye800CW secondary antibodies (1:15000, Life Technologies), signal was detected using LI-COR's Odyssey Infrared Imaging System with Odyssey Software. Values for protein signal intensity were obtained using Image Studio Lite Version4.0. Gli3 repressor

and full length protein levels and the Gli3 repressor/full length were compared between wild-type and mutant tissue using an unpaired t-test.

Scanning and transmission electron microscopy

TEM and SEM image acquisition were performed in the Cochin Imaging Facility and on the IBPS EM Facility, respectively. For scanning electron microscopy, embryos were dissected in 1.22x PBS (pH 7.4) and fixed overnight with 2% glutaraldehyde in 0.61x PBS (pH 7.4) at 4°C. Heads were then sectioned to separate the dorsal and ventral parts of the telencephalon, exposing their ventricular surfaces. Head samples were washed several times in 1.22x PBS and postfixed for 15 minutes in 1.22x PBS containing 1% OsO4. Fixed samples were washed several times in ultrapure water, dehydrated with a graded series of ethanol and prepared for scanning electron microscopy using the critical point procedure (CPD7501, Polaron). Their surfaces were coated with a 20 nm gold layer using a gold spattering device (Scancoat Six, Edwards). Samples were observed under a Cambridge S260 scanning electron microscope at 10 keV.

For transmission electron microscopy tissues were fixed for 1 hour with 3% glutaraldehyde, post-fixed in 1.22x PBS containing 1% OsO4, then dehydrated with a graded ethanol series. After 10 minutes in a 1:2 mixture of propane:epoxy resin, tissues were embedded in gelatin capsules with freshly prepared epoxy resin and polymerized at 60°C for 24 hours. Sections (80 nm) obtained using an ultramicrotome (Reichert Ultracut S) were stained with uranyl acetate and Reynold's lead citrate and observed with a Philips CM10 transmission electron microscope.

Statistical Analyses

Data were analysed using GraphPadPrism 8 software with n=3-8 embryos for all analyses. Shapiro-Wilk normality tests informed whether to use t-tests for normally distributed data and Mann Whitney tests for data which did not pass the normality test. Cortical thickness was analysed using a two way ANOVA followed by Sidak's multiple comparisons test. A fisher's exact test was used to analyse the quantification of normal and abnormal cilia. The Gli3 rescue experiments were evaluated with one way ANOVAS followed by Tukey's multiple comparisons test. A single asterisk indicates significance of $p<0.05$, two asterisks indicate significance of $p<0.01$ and three asterisks of $p<0.001$. Due to morphological changes blinding was not possible and scores were validated by a second independent observer. Supplementary Table 1 provides a summary of test statistics.

ACKNOWLEDGEMENTS

We are grateful to Drs Thomas Becker, Christos Gkogkas, John Mason, Pleasantine Mill, and David Price for critical comments on the manuscript, and Stéphane Schurmans for the *Inpp5e*$^{\Delta/+}$ mouse

line. We also thank Dr Michaël Trichet (electron microscopy platform of the IBPS-Sorbonne Universités Paris 6) and Dr Alain Schmitt (electron microscopy platform of the Institut Cochin CNRS-UMR 8104) for their help with scanning and transmission electron microscopy analyses, respectively. This work was supported by a grants from the Biotechnology and Biological Sciences Research Council (BB/P00122X/1) and from the Simons Initiative for the Developing Brain (SFARI -529085) to TT and from NIH R01GM095941 to JFR.

COMPETING INTERESTS

The authors declare no competing interests.

IMPACT STATEMENT:

Primary cilia mediated processing of the Gli3 transcription factor enables the formation of subtypes of projection neurons in appropriate numbers during the development of the cerebral cortex.

554 **REFERENCES**

555

556 Amaniti, E. M., Fu, C., Lewis, S., Saisana, M., Magnani, D., Mason, J. O., & Theil, T. (2015).
557 Expansion of the piriform cortex contributes to corticothalamic pathfinding defects in Gli3
558 conditional mutants. *Cereb Cortex, 25*(2), 460-471. doi:10.1093/cercor/bht244
559 Arai, Y., Pulvers, J. N., Haffner, C., Schilling, B., Nusslein, I., Calegari, F., & Huttner, W. B. (2011).
560 Neural stem and progenitor cells shorten S-phase on commitment to neuron production.
561 *Nature communications, 2*, 154. doi:10.1038/ncomms1155
562 Ariens-Kapers, C. U., Huber, G. C., & Crosby, E. C. (1936). The comparative anatomy of the
563 nervous system of the vertebrates including man. *New York Macmillan*.
564 Arnold, S. J., Huang, G. J., Cheung, A. F., Era, T., Nishikawa, S., Bikoff, E. K., . . . Groszer, M.
565 (2008). The T-box transcription factor Eomes/Tbr2 regulates neurogenesis in the cortical
566 subventricular zone. *Genes Dev, 22*(18), 2479-2484. doi:10.1101/gad.475408
567 Ashique, A. M., Choe, Y., Karlen, M., May, S. R., Phamluong, K., Solloway, M. J., . . . Peterson, A.
568 S. (2009). The Rfx4 transcription factor modulates Shh signaling by regional control of
569 ciliogenesis. *Sci Signal, 2*(95), ra70. doi:10.1126/scisignal.2000602
570 Benadiba, C., Magnani, D., Niquille, M., Morle, L., Valloton, D., Nawabi, H., . . . Durand, B. (2012).
571 The ciliogenic transcription factor RFX3 regulates early midline distribution of guidepost
572 neurons required for corpus callosum development. *PLoS genetics, 8*(3), e1002606.
573 doi:10.1371/journal.pgen.1002606
574 Besse, L., Neti, M., Anselme, I., Gerhardt, C., Ruther, U., Laclef, C., & Schneider-Maunoury, S.
575 (2011). Primary cilia control telencephalic patterning and morphogenesis via Gli3
576 proteolytic processing. *Development, 138*(10), 2079-2088. doi:10.1242/dev.059808
577 Bielas, S. L., Silhavy, J. L., Brancati, F., Kisseleva, M. V., Al-Gazali, L., Sztriha, L., . . . Gleeson, J.
578 G. (2009). Mutations in INPP5E, encoding inositol polyphosphate-5-phosphatase E, link
579 phosphatidyl inositol signaling to the ciliopathies. *Nat Genet, 41*(9), 1032-1036.
580 doi:10.1038/ng.423
581 Böse, J., Grotewold, L., & Rüther, U. (2002). Pallister-Hall syndrome phenotype in mice mutant for
582 Gli3. *Hum Mol Genet, 11*(9), 1129-1135.
583 Bulfone, A., Puelles, L., Porteus, M. H., Frohman, M. A., Martin, G. R., & Rubenstein, J. L. (1993).
584 Spatially restricted expression of Dlx-1, Dlx-2 (Tes-1), Gbx-2, and Wnt-3 in the embryonic
585 day 12.5 mouse forebrain defines potential transverse and longitudinal segmental
586 boundaries. *J Neurosci, 13*(7), 3155-3172.
587 Cardenas, A., Villalba, A., de Juan Romero, C., Pico, E., Kyrousi, C., Tzika, A. C., . . . Borrell, V.
588 (2018). Evolution of Cortical Neurogenesis in Amniotes Controlled by Robo Signaling
589 Levels. *Cell, 174*(3), 590-606 e521. doi:10.1016/j.cell.2018.06.007
590 Caspary, T., Larkins, C. E., & Anderson, K. V. (2007). The graded response to Sonic Hedgehog
591 depends on cilia architecture. *Developmental cell, 12*(5), 767-778.
592 doi:10.1016/j.devcel.2007.03.004
593 Chavez, M., Ena, S., Van Sande, J., de Kerchove d'Exaerde, A., Schurmans, S., & Schiffmann, S.
594 N. (2015). Modulation of Ciliary Phosphoinositide Content Regulates Trafficking and Sonic
595 Hedgehog Signaling Output. *Developmental cell, 34*(3), 338-350.
596 doi:10.1016/j.devcel.2015.06.016
597 Dyson, J. M., Conduit, S. E., Feeney, S. J., Hakim, S., DiTommaso, T., Fulcher, A. J., . . . Mitchell,
598 C. A. (2017). INPP5E regulates phosphoinositide-dependent cilia transition zone function. *J*
599 *Cell Biol, 216*(1), 247-263. doi:10.1083/jcb.201511055
600 Englund, C., Fink, A., Lau, C., Pham, D., Daza, R. A., Bulfone, A., . . . Hevner, R. F. (2005). Pax6,
601 Tbr2, and Tbr1 are expressed sequentially by radial glia, intermediate progenitor cells, and
602 postmitotic neurons in developing neocortex. *J Neurosci, 25*(1), 247-251.
603 Florio, M., & Huttner, W. B. (2014). Neural progenitors, neurogenesis and the evolution of the
604 neocortex. *Development, 141*(11), 2182-2194. doi:10.1242/dev.090571
605 Foerster, P., Daclin, M., Asm, S., Faucourt, M., Boletta, A., Genovesio, A., & Spassky, N. (2017).
606 mTORC1 signaling and primary cilia are required for brain ventricle morphogenesis.
607 *Development, 144*(2), 201-210. doi:10.1242/dev.138271

Fotaki, V., Yu, T., Zaki, P. A., Mason, J. O., & Price, D. J. (2006). Abnormal positioning of diencephalic cell types in neocortical tissue in the dorsal telencephalon of mice lacking functional Gli3. *J Neurosci, 26*(36), 9282-9292.

Frantz, G. D., Bohner, A. P., Akers, R. M., & McConnell, S. K. (1994). Regulation of the POU domain gene SCIP during cerebral cortical development. *J Neurosci, 14*(2), 472-485.

Galceran, J., Miyashita-Lin, E. M., Devaney, E., Rubenstein, J. L., & Grosschedl, R. (2000). Hippocampus development and generation of dentate gyrus granule cells is regulated by LEF1. *Development, 127*(3), 469-482.

Garcia-Gonzalo, F. R., Corbit, K. C., Sirerol-Piquer, M. S., Ramaswami, G., Otto, E. A., Noriega, T. R., . . . Reiter, J. F. (2011). A transition zone complex regulates mammalian ciliogenesis and ciliary membrane composition. *Nat Genet, 43*(8), 776-784. doi:10.1038/ng.891

Garcia-Gonzalo, F. R., Phua, S. C., Roberson, E. C., Garcia, G., 3rd, Abedin, M., Schurmans, S., . . . Reiter, J. F. (2015). Phosphoinositides Regulate Ciliary Protein Trafficking to Modulate Hedgehog Signaling. *Developmental cell, 34*(4), 400-409. doi:10.1016/j.devcel.2015.08.001

Gerhardt, C., Lier, J. M., Burmuhl, S., Struchtrup, A., Deutschmann, K., Vetter, M., . . . Ruther, U. (2015). The transition zone protein Rpgrip1l regulates proteasomal activity at the primary cilium. *J Cell Biol, 210*(1), 115-133. doi:10.1083/jcb.201408060

Gladwyn-Ng, I., Cordon-Barris, L., Alfano, C., Creppe, C., Couderc, T., Morelli, G., . . . Nguyen, L. (2018). Stress-induced unfolded protein response contributes to Zika virus-associated microcephaly. *Nature neuroscience, 21*(1), 63-71. doi:10.1038/s41593-017-0038-4

Götz, M., Stoykova, A., & Gruss, P. (1998). Pax6 controls radial glia differentiation in the cerebral cortex. *Neuron, 21*(5), 1031-1044.

Gradwohl, G., Fode, C., & Guillemot, F. (1996). Restricted expression of a novel murine atonal-related bHLH protein in undifferentiated neural precursors. *Dev Biol, 180*(1), 227-241.

Grove, E. A., Tole, S., Limon, J., Yip, L., & Ragsdale, C. W. (1998). The hem of the embryonic cerebral cortex is defined by the expression of multiple Wnt genes and is compromised in Gli3-deficient mice. *Development, 125*(12), 2315-2325.

Gupta, A., Fabian, L., & Brill, J. A. (2018). Phosphatidylinositol 4,5-bisphosphate regulates cilium transition zone maturation in Drosophila melanogaster. *J Cell Sci, 131*(16). doi:10.1242/jcs.218297

Hall, P. A., Levison, D. A., Woods, A. L., Yu, C. C., Kellock, D. B., Watkins, J. A., . . . et al. (1990). Proliferating cell nuclear antigen (PCNA) immunolocalization in paraffin sections: an index of cell proliferation with evidence of deregulated expression in some neoplasms. *J Pathol, 162*(4), 285-294. doi:10.1002/path.1711620403

Hasenpusch-Theil, K., West, S., Kelman, A., Kozic, Z., Horrocks, S., McMahon, A. P., . . . Theil, T. (2018). Gli3 controls the onset of cortical neurogenesis by regulating the radial glial cell cycle through Cdk6 expression. *Development, 145*(17). doi:10.1242/dev.163147

Haubensak, W., Attardo, A., Denk, W., & Huttner, W. B. (2004). Neurons arise in the basal neuroepithelium of the early mammalian telencephalon: a major site of neurogenesis. *Proc Natl Acad Sci U S A, 101*(9), 3196-3201.

Hill, R. E., Jones, P. F., Rees, A. R., Sime, C. M., Justice, M. J., Copeland, N. G., . . . Davidson, D. R. (1989). A new family of mouse homeo box-containing genes: molecular structure, chromosomal location, and developmental expression of Hox-7.1. *Genes Dev, 3*(1), 26-37.

Hui, C. C., Slusarski, D., Platt, K. A., Holmgren, R., & Joyner, A. L. (1994). Expression of three mouse homologs of the Drosophila segment polarity gene cubitus interruptus, Gli, Gli-2, and Gli-3, in ectoderm- and mesoderm-derived tissues suggests multiple roles during postimplantation development. *Dev Biol, 162*(2), 402-413.

Jacoby, M., Cox, J. J., Gayral, S., Hampshire, D. J., Ayub, M., Blockmans, M., . . . Schurmans, S. (2009). INPP5E mutations cause primary cilium signaling defects, ciliary instability and ciliopathies in human and mouse. *Nat Genet, 41*(9), 1027-1031.

Johnson, D. R. (1967). Extra-toes: a new mutant gene causing multiple abnormalities in the mouse. *J Embryol Exp Morphol, 17*(3), 543-581.

Jones, C. M., Lyons, K. M., & Hogan, B. L. (1991). Involvement of Bone Morphogenetic Protein-4 (BMP-4) and Vgr-1 in morphogenesis and neurogenesis in the mouse. *Development, 111*(2), 531-542.

Kisseleva, M. V., Cao, L., & Majerus, P. W. (2002). Phosphoinositide-specific inositol polyphosphate 5-phosphatase IV inhibits Akt/protein kinase B phosphorylation and leads to apoptotic cell death. *J Biol Chem, 277*(8), 6266-6272. doi:10.1074/jbc.M105969200

Laclef, C., Anselme, I., Besse, L., Catala, M., Palmyre, A., Baas, D., . . . Schneider-Maunoury, S. (2015). The role of primary cilia in corpus callosum formation is mediated by production of the Gli3 repressor. *Hum Mol Genet, 24*(17), 4997-5014. doi:10.1093/hmg/ddv221

Laguesse, S., Creppe, C., Nedialkova, D. D., Prevot, P. P., Borgs, L., Huysseune, S., . . . Nguyen, L. (2015). A Dynamic Unfolded Protein Response Contributes to the Control of Cortical Neurogenesis. *Developmental cell, 35*(5), 553-567. doi:10.1016/j.devcel.2015.11.005

Lee, S. M., Tole, S., Grove, E., & McMahon, A. P. (2000). A local Wnt-3a signal is required for development of the mammalian hippocampus. *Development, 127*(3), 457-467.

Liem, K. F., Jr., Tremml, G., & Jessell, T. M. (1997). A role for the roof plate and its resident TGFbeta-related proteins in neuronal patterning in the dorsal spinal cord. *Cell, 91*(1), 127-138.

Lustig, B., Jerchow, B., Sachs, M., Weiler, S., Pietsch, T., Karsten, U., . . . Behrens, J. (2002). Negative Feedback Loop of Wnt Signaling through Upregulation of Conductin/Axin2 in Colorectal and Liver Tumors. *Mol. Cell. Biol., 22*(4), 1184-1193.

Magnani, D., Hasenpusch-Theil, K., Benadiba, C., Yu, T., Basson, M. A., Price, D. J., . . . Theil, T. (2014). Gli3 controls corpus callosum formation by positioning midline guideposts during telencephalic patterning. *Cerebral cortex, 24*(1), 186-198. doi:10.1093/cercor/bhs303

Magnani, D., Hasenpusch-Theil, K., Jacobs, E. C., Campagnoni, A. T., Price, D. J., & Theil, T. (2010). The Gli3 hypomorphic mutation Pdn causes selective impairment in the growth, patterning, and axon guidance capability of the lateral ganglionic eminence. *J Neurosci, 30*(41), 13883-13894. doi:30/41/13883 [pii]
10.1523/JNEUROSCI.3650-10.2010

Magnani, D., Morle, L., Hasenpusch-Theil, K., Paschaki, M., Jacoby, M., Schurmans, S., . . . Theil, T. (2015). The ciliogenic transcription factor Rfx3 is required for the formation of the thalamocortical tract by regulating the patterning of prethalamus and ventral telencephalon. *Hum Mol Genet, 24*(9), 2578-2593. doi:10.1093/hmg/ddv021

Mao, H., Tang, Z., Li, H., Sun, B., Tan, M., Fan, S., . . . Sun, Y. (2019). Neddylation inhibitor MLN4924 suppresses cilia formation by modulating AKT1. *Protein Cell*. doi:10.1007/s13238-019-0614-3

Martinez-Cerdeno, V., Noctor, S. C., & Kriegstein, A. R. (2006). The role of intermediate progenitor cells in the evolutionary expansion of the cerebral cortex. *Cereb Cortex, 16 Suppl 1*, i152-161. doi:10.1093/cercor/bhk017

Martynoga, B., Morrison, H., Price, D. J., & Mason, J. O. (2005). Foxg1 is required for specification of ventral telencephalon and region-specific regulation of dorsal telencephalic precursor proliferation and apoptosis. *Dev Biol, 283*(1), 113-127.

Miyata, T., Kawaguchi, A., Saito, K., Kawano, M., Muto, T., & Ogawa, M. (2004). Asymmetric production of surface-dividing and non-surface-dividing cortical progenitor cells. *Development, 131*(13), 3133-3145. doi:10.1242/dev.01173

Noctor, S. C., Martinez-Cerdeno, V., Ivic, L., & Kriegstein, A. R. (2004). Cortical neurons arise in symmetric and asymmetric division zones and migrate through specific phases. *Nature neuroscience, 7*(2), 136-144. doi:10.1038/nn1172

Nowakowski, R. S., Lewin, S. B., & Miller, M. W. (1989). Bromodeoxyuridine immunohistochemical determination of the lengths of the cell cycle and the DNA-synthetic phase for an anatomically defined population. *J Neurocytol, 18*(3), 311-318.

Oliver, G., Sosa-Pineda, B., Geisendorf, S., Spana, E. P., Doe, C. Q., & Gruss, P. (1993). Prox 1, a prospero-related homeobox gene expressed during mouse development. *Mech Dev, 44*(1), 3-16. doi:10.1016/0925-4773(93)90012-m

Parthasarathy, S., Srivatsa, S., Nityanandam, A., & Tarabykin, V. (2014). Ntf3 acts downstream of Sip1 in cortical postmitotic neurons to control progenitor cell fate through feedback signaling. *Development, 141*(17), 3324-3330. doi:10.1242/dev.114173

Petrova, R., Garcia, A. D., & Joyner, A. L. (2013). Titration of GLI3 repressor activity by sonic hedgehog signaling is critical for maintaining multiple adult neural stem cell and astrocyte

functions. *The Journal of neuroscience : the official journal of the Society for Neuroscience, 33*(44), 17490-17505. doi:10.1523/JNEUROSCI.2042-13.2013
Plotnikova, O. V., Seo, S., Cottle, D. L., Conduit, S., Hakim, S., Dyson, J. M., . . . Smyth, I. M. (2015). INPP5E interacts with AURKA, linking phosphoinositide signaling to primary cilium stability. *J Cell Sci, 128*(2), 364-372. doi:10.1242/jcs.161323
Poretti, A., Huisman, T. A., Scheer, I., & Boltshauser, E. (2011). Joubert syndrome and related disorders: spectrum of neuroimaging findings in 75 patients. *AJNR Am J Neuroradiol, 32*(8), 1459-1463. doi:10.3174/ajnr.A2517
Postel, M., Karam, A., Pezeron, G., Schneider-Maunoury, S., & Clement, F. (2019). A multiscale mathematical model of cell dynamics during neurogenesis in the mouse cerebral cortex. *BMC Bioinformatics, 20*(1), 470. doi:10.1186/s12859-019-3018-8
Postiglione, M. P., Juschke, C., Xie, Y., Haas, G. A., Charalambous, C., & Knoblich, J. A. (2011). Mouse inscuteable induces apical-basal spindle orientation to facilitate intermediate progenitor generation in the developing neocortex. *Neuron, 72*(2), 269-284. doi:10.1016/j.neuron.2011.09.022
Putoux, A., Baas, D., Paschaki, M., Morle, L., Maire, C., Attie-Bitach, T., . . . Durand, B. (2019). Altered GLI3 and FGF8 signaling underlies acrocallosal syndrome phenotypes in Kif7 depleted mice. *Hum Mol Genet, 28*(6), 877-887. doi:10.1093/hmg/ddy392
Rallu, M., Machold, R., Gaiano, N., Corbin, J. G., McMahon, A. P., & Fishell, G. (2002). Dorsoventral patterning is established in the telencephalon of mutants lacking both Gli3 and Hedgehog signaling. *Development, 129*(21), 4963-4974.
Rash, B. G., & Grove, E. A. (2007). Patterning the dorsal telencephalon: a role for sonic hedgehog? *J Neurosci, 27*(43), 11595-11603.
Reiter, J. F., & Skarnes, W. C. (2006). Tectonic, a novel regulator of the Hedgehog pathway required for both activation and inhibition. *Genes Dev, 20*(1), 22-27. doi:10.1101/gad.1363606
Sang, L., Miller, J. J., Corbit, K. C., Giles, R. H., Brauer, M. J., Otto, E. A., . . . Jackson, P. K. (2011). Mapping the NPHP-JBTS-MKS protein network reveals ciliopathy disease genes and pathways. *Cell, 145*(4), 513-528. doi:10.1016/j.cell.2011.04.019
Seuntjens, E., Nityanandam, A., Miquelajauregui, A., Debruyn, J., Stryjewska, A., Goebbels, S., . . . Tarabykin, V. (2009). Sip1 regulates sequential fate decisions by feedback signaling from postmitotic neurons to progenitors. *Nature neuroscience, 12*(11), 1373-1380. doi:10.1038/nn.2409
Shi, X., Garcia, G., 3rd, Van De Weghe, J. C., McGorty, R., Pazour, G. J., Doherty, D., . . . Reiter, J. F. (2017). Super-resolution microscopy reveals that disruption of ciliary transition-zone architecture causes Joubert syndrome. *Nat Cell Biol, 19*(10), 1178-1188. doi:10.1038/ncb3599
Silva, C. G., Peyre, E., & Nguyen, L. (2019). Cell migration promotes dynamic cellular interactions to control cerebral cortex morphogenesis. *Nat Rev Neurosci, 20*(6), 318-329. doi:10.1038/s41583-019-0148-y
Simeone, A., Gulisano, M., Acampora, D., Stornaiuolo, A., Rambaldi, M., & Boncinelli, E. (1992). Two vertebrate homeobox genes related to the Drosophila empty spiracles gene are expressed in the embryonic cerebral cortex. *EMBO J, 11*(7), 2541-2550.
Theil, T. (2005). Gli3 is required for the specification and differentiation of preplate neurons. *Dev Biol, 286*(2), 559-571.
Theil, T., Alvarez-Bolado, G., Walter, A., & Rüther, U. (1999). Gli3 is required for Emx gene expression during dorsal telencephalon development. *Development, 126*(16), 3561-3571.
Thomas, S., Legendre, M., Saunier, S., Bessieres, B., Alby, C., Bonniere, M., . . . Attie-Bitach, T. (2012). TCTN3 mutations cause Mohr-Majewski syndrome. *Am J Hum Genet, 91*(2), 372-378. doi:10.1016/j.ajhg.2012.06.017
Uzquiano, A., Cifuentes-Diaz, C., Jabali, A., Romero, D. M., Houllier, A., Dingli, F., . . . Francis, F. (2019). Mutations in the Heterotopia Gene Eml1/EML1 Severely Disrupt the Formation of Primary Cilia. *Cell Rep, 28*(6), 1596-1611 e1510. doi:10.1016/j.celrep.2019.06.096
Valente, E. M., Rosti, R. O., Gibbs, E., & Gleeson, J. G. (2014). Primary cilia in neurodevelopmental disorders. *Nat Rev Neurol, 10*(1), 27-36. doi:10.1038/nrneurol.2013.247

774 Vasistha, N. A., Garcia-Moreno, F., Arora, S., Cheung, A. F., Arnold, S. J., Robertson, E. J., &
775 Molnar, Z. (2015). Cortical and Clonal Contribution of Tbr2 Expressing Progenitors in the
776 Developing Mouse Brain. *Cereb Cortex, 25*(10), 3290-3302. doi:10.1093/cercor/bhu125
777 Walther, C., & Gruss, P. (1991). Pax-6, a murine paired box gene, is expressed in the developing
778 CNS. *Development, 113*(4), 1435-1449.
779 Wang, C., Li, J., Meng, Q., & Wang, B. (2017). Three Tctn proteins are functionally conserved in
780 the regulation of neural tube patterning and Gli3 processing but not ciliogenesis and
781 Hedgehog signaling in the mouse. *Dev Biol, 430*(1), 156-165.
782 doi:10.1016/j.ydbio.2017.08.003
783 Wang, H., Ge, G., Uchida, Y., Luu, B., & Ahn, S. (2011). Gli3 is required for maintenance and fate
784 specification of cortical progenitors. *J Neurosci, 31*(17), 6440-6448. doi:31/17/6440 [pii]
785 10.1523/JNEUROSCI.4892-10.2011
786 Wang, H., Kane, A. W., Lee, C., & Ahn, S. (2014). Gli3 repressor controls cell fates and cell
787 adhesion for proper establishment of neurogenic niche. *Cell Rep, 8*(4), 1093-1104.
788 doi:10.1016/j.celrep.2014.07.006
789 Wang, W., Jossin, Y., Chai, G., Lien, W. H., Tissir, F., & Goffinet, A. M. (2016). Feedback
790 regulation of apical progenitor fate by immature neurons through Wnt7-Celsr3-Fzd3
791 signalling. *Nature communications, 7*, 10936. doi:10.1038/ncomms10936
792 Warren, N., Caric, D., Pratt, T., Clausen, J. A., Asavaritikrai, P., Mason, J. O., . . . Price, D. J.
793 (1999). The transcription factor, Pax6, is required for cell proliferation and differentiation in
794 the developing cerebral cortex. *Cereb Cortex, 9*(6), 627-635.
795 Wiegering, A., Petzsch, P., Kohrer, K., Ruther, U., & Gerhardt, C. (2019). GLI3 repressor but not
796 GLI3 activator is essential for mouse eye patterning and morphogenesis. *Dev Biol, 450*(2),
797 141-154. doi:10.1016/j.ydbio.2019.02.018
798 Willaredt, M. A., Hasenpusch-Theil, K., Gardner, H. A., Kitanovic, I., Hirschfeld-Warneken, V. C.,
799 Gojak, C. P., . . . Tucker, K. L. (2008). A crucial role for primary cilia in cortical
800 morphogenesis. *J Neurosci, 28*(48), 12887-12900.
801 Wilson, S. L., Wilson, J. P., Wang, C., Wang, B., & McConnell, S. K. (2012). Primary cilia and Gli3
802 activity regulate cerebral cortical size. *Dev Neurobiol, 72*(9), 1196-1212.
803 doi:10.1002/dneu.20985
804 Yee, L. E., Garcia-Gonzalo, F. R., Bowie, R. V., Li, C., Kennedy, J. K., Ashrafi, K., . . . Reiter, J. F.
805 (2015). Conserved Genetic Interactions between Ciliopathy Complexes Cooperatively
806 Support Ciliogenesis and Ciliary Signaling. *PLoS Genet, 11*(11), e1005627.
807 doi:10.1371/journal.pgen.1005627
808 Yu, J. S., & Cui, W. (2016). Proliferation, survival and metabolism: the role of PI3K/AKT/mTOR
809 signalling in pluripotency and cell fate determination. *Development, 143*(17), 3050-3060.
810 doi:10.1242/dev.137075
811 Yun, K., Potter, S., & Rubenstein, J. L. (2001). Gsh2 and Pax6 play complementary roles in
812 dorsoventral patterning of the mammalian telencephalon. *Development, 128*(2), 193-205.
813 Zhang, Y., Liu, G., Guo, T., Liang, X. G., Du, H., Yang, L., . . . Chen, B. (2020). Cortical Neural
814 Stem Cell Lineage Progression Is Regulated by Extrinsic Signaling Molecule Sonic
815 Hedgehog. *Cell Rep, 30*(13), 4490-4504 e4494. doi:10.1016/j.celrep.2020.03.027
816
817

FIGURES AND FIGURE LEGENDS

Figure 1

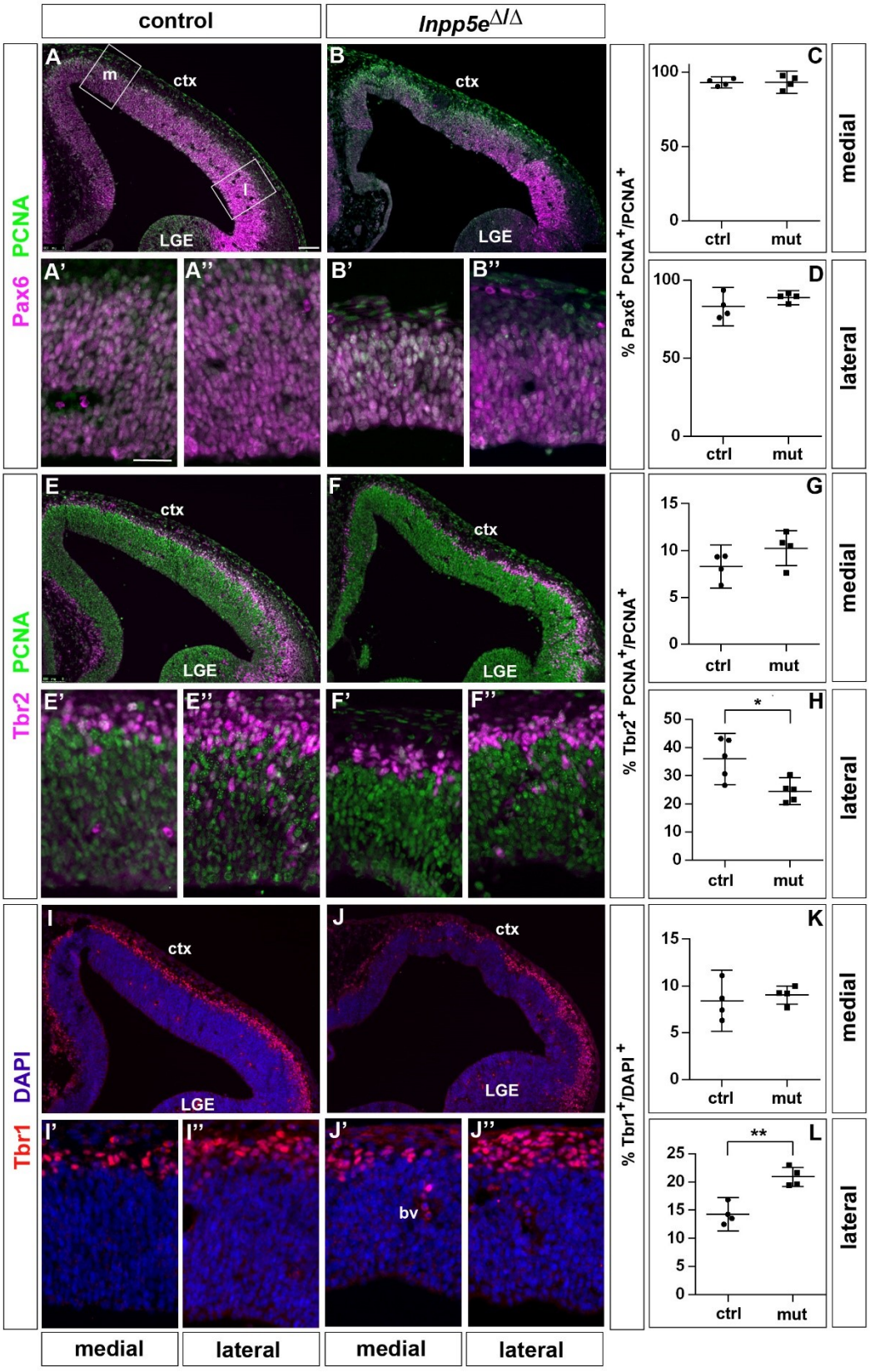

Figure 1: Increased neuron formation in the dorsolateral telencephalon of E12.5 *Inpp5*$^{\Delta/\Delta}$ embryos. (A-D) Pax6/PCNA double immunofluorescence staining revealed the proportion of apical

822 radial glial cells which remained unaltered in the mutant. The boxes in (A) indicate the regions in the
823 medial (m) and lateral (l) telencephalon at which cell counts were performed. (E-H) Reduced
824 proportions of basal progenitors in the lateral telencephalon as revealed by staining for Tbr2 and
825 PCNA. (I-L) Tbr1 immunostaining showed that the proportion of neurons is increased in the lateral
826 telencephalon. (A-J) The insets labelled with ‘ and ‘’ are representative magnifications of medial and
827 lateral levels, respectively. All statistical data are presented as means ± 95% confidence intervals
828 (CI); unpaired t-tests; n = 4 except for (H) with n=5; * $p < 0.05$; ** $p < 0.01$. Scale bar: 100μm (A) and
829 50μm (A’). ctx: cortex; LGE: lateral ganglionic eminence.
830

Figure 2

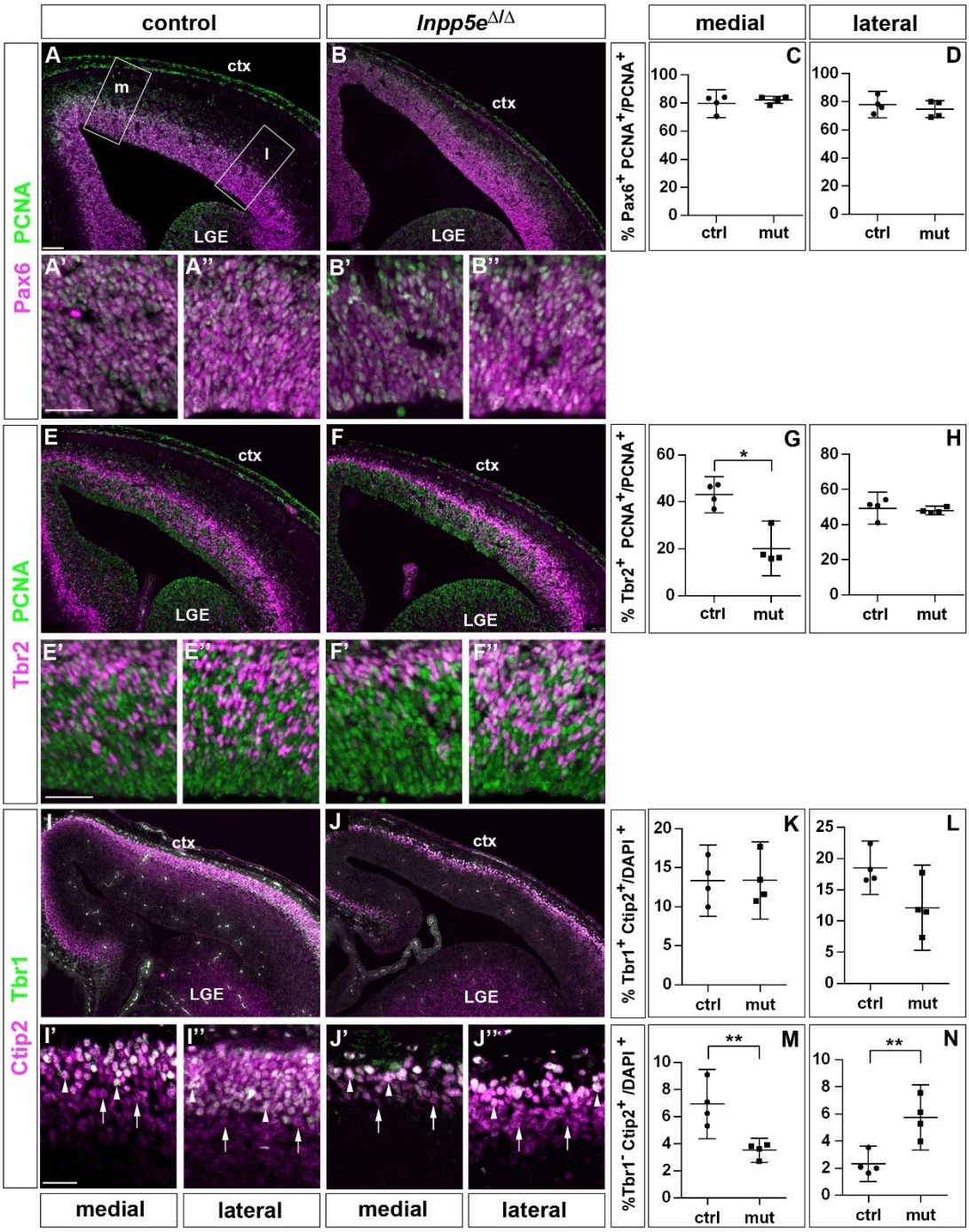

Figure 2: Proportions of radial glial cells, basal progenitors and neurons in the neocortex of E14.5 *Inpp5e*$^{\Delta/\Delta}$ embryos. (A-D) The proportion of radial glial cells remains unaffected by the *Inpp5e* mutation as revealed by Pax6/PCNA double immunofluorescence. The boxes in A indicate the regions in the medial (m) and lateral (l) telencephalon at which cell counts were performed. (E-H) Tbr2/PCNA double staining showed a reduced proportion of basal progenitors in the *Inpp5e*$^{\Delta/\Delta}$ medial but not lateral neocortex. (I-N) The proportion of Tbr1+Ctip2+ neurons is not significantly altered (I-

838 L) whereas the proportion of Tbr1-Ctip2+ neurons is decreased and increased in the medial and
839 lateral neocortex, respectively. Arrows in (I and J) label Tbr1-Ctip2+ neurons and arrowheads
840 Tbr1+Ctip2+ neurons. (A-J) The insets labelled with ‘ and ‘’ are representative magnifications of
841 medial and lateral levels, respectively. All statistical data are presented as means ± 95% confidence
842 intervals (CI); Unpaired t-tests (C, D, H, K-N) and Mann Whitney test (G); n = 4; * $p < 0.05$; ** $p <$
843 0.01. Scale bars: 100μm (A) and 50μm (A’, E’ and I’). ctx: cortex; LGE: lateral ganglionic eminence.
844

Figure 3

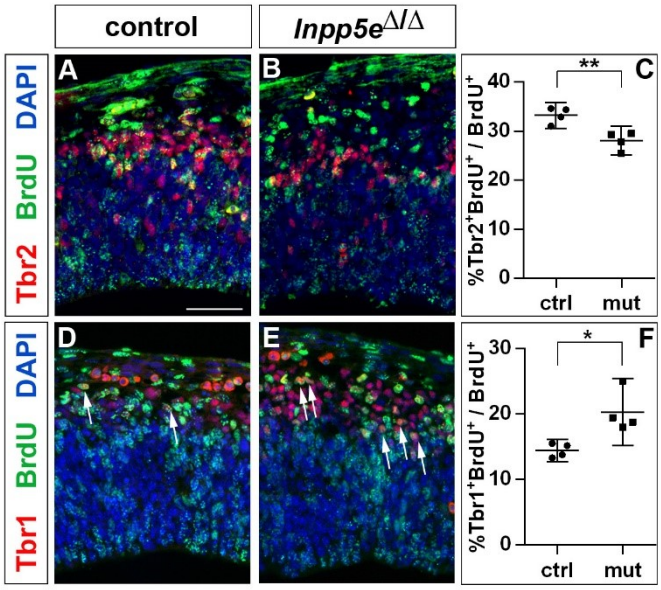

Figure 3: Increased neurogenesis at the expense of basal progenitor formation in the E12.5 *Inpp5e*$^{\Delta/\Delta}$ mutant lateral telencephalon. Immunohistochemistry on sections of E12.5 control (A, D) and *Inpp5e*$^{\Delta/\Delta}$ embryos (B, E) that were treated with BrdU 24 hours earlier. (A-C) Tbr2/BrdU double labelling showed that less basal progenitors formed from the BrdU labelled progenitor cohort in *Inpp5e*$^{\Delta/\Delta}$ embryos. (D-F) The proportion of newly formed Tbr1+ neurons was increased in *Inpp5e*$^{\Delta/\Delta}$ embryos. The arrows in D and E label Tbr1^{+}BrdU^{+} cells. All statistical data are presented as means ± 95% confidence intervals (CI); unpaired t tests; n = 4; * $p < 0.05$; ** $p < 0.01$. Scale bar: 50μm.

Figure 4

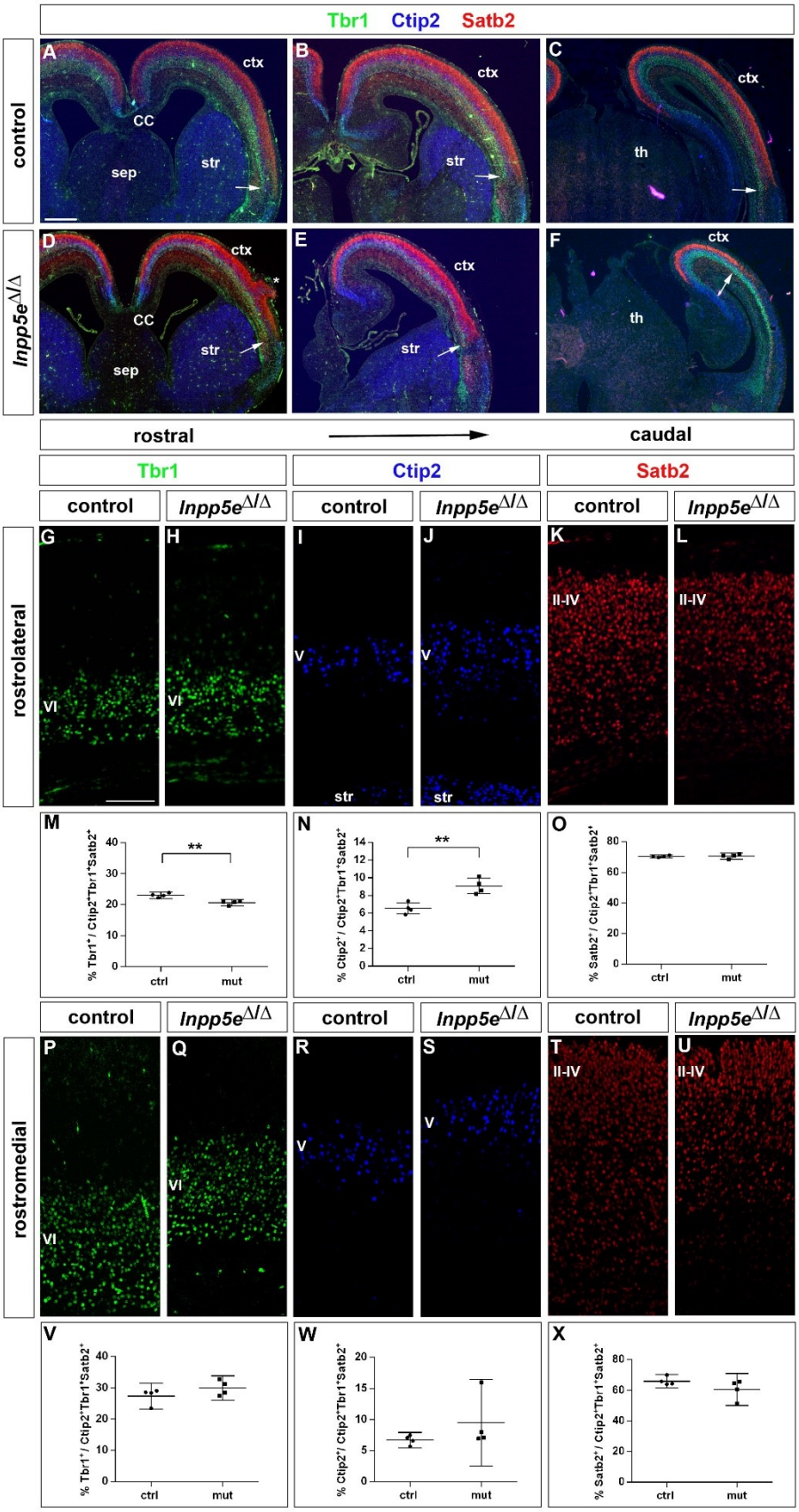
Tbr1 Ctip2 Satb2
control
Inpp5e Δ/Δ
A
B
C
D
E
F
ctx
CC
sep
str
th
rostral
caudal
Tbr1
Ctip2
Satb2
control
Inpp5e Δ/Δ
rostrolateral
rostromedial
G
H
I
J
K
L
M
N
O
P
Q
R
S
T
U
V
W
X
VI
V
II-IV
% Tbr1+ / Ctip2+Tbr1+Satb2+
% Ctip2+ / Ctip2+Tbr1+Satb2+
% Satb2+ / Ctip2+Tbr1+Satb2+
ctrl
mut
**

854

Figure 4: Increased formation of layer V neurons in E18.5 *Inpp5e*$^{\Delta/\Delta}$ mutants. (A-F) Coronal sections immunostained for the deep layer markers Tbr1 (layer VI) and Ctip2 (layer V) and for the upper layer marker Satb2 (layers II-IV); there is no obvious defect in layering in *Inpp5e*$^{\Delta/\Delta}$ embryos except for the formation of a heterotopia (asterisk in D). At caudal levels, the cortex becomes thinner and the rhinal fissure is shifted medially as indicated by the arrows. (G-O) Formation of cortical neurons at rostrolateral levels. The proportion of Tbr1+layer VI neurons is decreased with a concomitant increase in Ctip2+layer V neurons. (P-X) Portion of cortical neurons at rostromedial levels. Immunolabeling with cortical layer markers revealed no significant difference. Note that due to the thinner cortex, the position of layer VI Tbr1+ (Q) and layer V Ctip2+ neurons (J, S) appears to be shifted to more superficial positions, however, the relative order of these layers remains unaffected. All statistical data are presented as means ± 95% confidence intervals (CI); unpaired t-tests (M-O, X); Mann Whitney tests (V, W); n = 4; ** $p < 0.01$. Scale bars: 500μm (A) and 100μm (G). CC: corpus callosum; ctx: cortex; sep: septum; str: striatum.

Figure 5

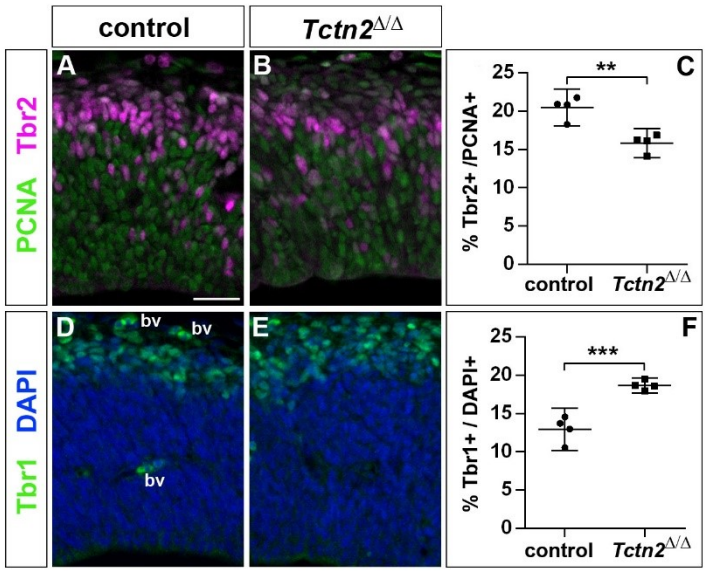

Figure 5: Increased generation of cortical neurons in the lateral neocortex of E12.5 *Tctn2*$^{\Delta/\Delta}$ embryos. (A-C) Double immunofluorescence for PCNA and Tbr2 revealed a significantly decreased proportion of basal progenitors. (D-F) The portion of Tbr1^{+} cortical neurons was increased. All statistical data are presented as means ± 95% confidence intervals (CI); unpaired t tests; n = 4; ** p < 0.01; *** p < 0.001. Scale bar: 50μm. bv: blood vessel.

Figure 6

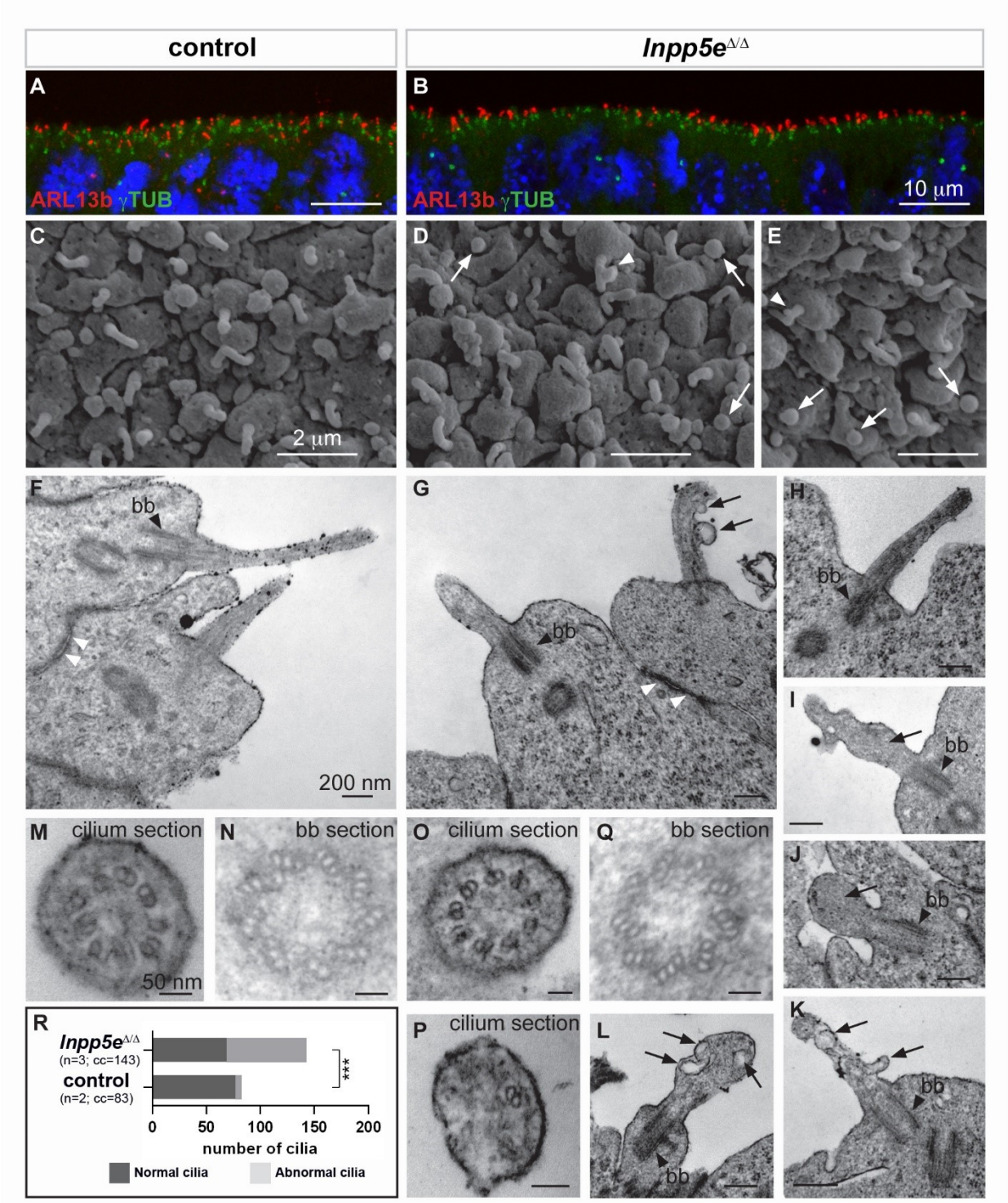

Figure 6: Ciliary defects in E12.5 *Inpp5e*$^{\Delta/\Delta}$ forebrain. (A-B) Immunohistochemistry for Arl13b and γ-Tubulin (γTUB) on E12.5 brain cryosections showed an accumulation of ciliary axonemes and basal bodies, respectively, at the apical border of radial glial cells facing the ventricules in both control (A) and *Inpp5e*$^{\Delta/\Delta}$ (B) embryos without any gross difference. Scale bars: 10 μm.

(C-E) Scanning electron microscopy (SEM) on E12.5 control (C) and *Inpp5e*$^{\Delta/\Delta}$ (D, E) brains highlighted the presence of primary cilia projecting from the apical surface of radial glial cells in both control (A) and *Inpp5e*$^{\Delta/\Delta}$ (B) embryos. However, SEM also revealed the presence of abnormal cilia in *Inpp5e*$^{\Delta/\Delta}$ embryos having a spherical shape (arrows in D and E) or aberrant lateral buddings (arrowheads in D and E). Scale bars: 2 μm. (F-L) Transmission electron microscopy (TEM) analysis on E12.5 brains showed longitudinal sections of primary cilia in control (F) and *Inpp5e*$^{\Delta/\Delta}$ (G-L) embryos. In control primary cilia, the axoneme appeared as an extension of the basal body (bb, black arrowheards) (F-H). In addition to cilia with normal morphology, abnormal cilia were identified in *Inpp5e*$^{\Delta/\Delta}$ embryos thanks to the presence of a basal body apparently correctly docked to the apical membrane. Abnormal cilia lacked an axoneme (I, J, L) or showed unusual membranous structures, such as budding (G, K) or internal (I, K, L) vesicles (arrows) or undulating peripheral membranes (I). Note that tight junctions (white arrowheads in F and G) appeared normal in *Inpp5e*$^{\Delta/\Delta}$ (G) and control (F) embryos, suggesting that apico-basal polarity of *Inpp5e*$^{\Delta/\Delta}$ radial glial cells was not compromised. Scale bars: 200 nm. (M-Q) TEM images showing transverse sections of the axoneme (M, O, P) and the basal body (N, Q) in control (M, N) and *Inpp5e*$^{\Delta/\Delta}$ (O-Q) embryos with no major difference in the basal bodies between control (N) and *Inpp5e*$^{\Delta/\Delta}$ (Q) embryos. However, transverse section of primary cilia in *Inpp5e*$^{\Delta/\Delta}$ brains revealed the presence of normal axonemes composed of 9 correctly organized doublets of microtubules on some radial glial cells (O), while others harboured an abnormal axoneme containing a lower number of microtubule doublets (P). Scale bars: 50 nm. (R) Graph showing the number of normal versus abnormal cilia (cil.) found on TEM images from control (n=3) or *Inpp5e*$^{\Delta/\Delta}$ (n=3) embryos. cc: counted cilia.

Figure 7

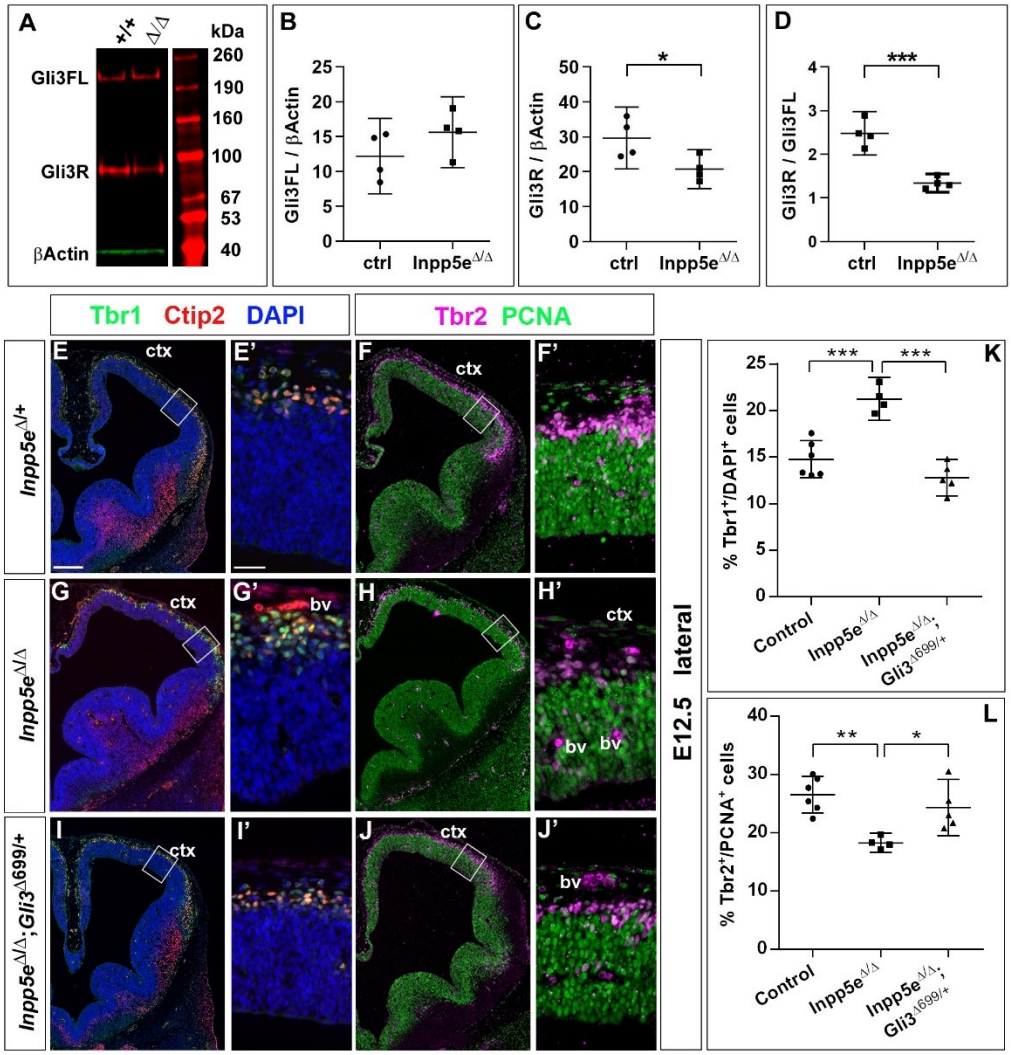

Figure 7: Re-introducing a single copy of the Gli3 repressor rescues the neurogenesis defect in E12.5 *Inpp5e* mutants. (A-D). Gli3 Western blot on E12.5 dorsal telencephalic tissue revealed the Gli3 full length (FL) and repressor (R) forms (A). While Gli3FL levels are not affected (B), levels of Gli3R (C) and the Gli3R/Gli3FL ratio (D) are decreased in *Inpp5e*$^{\Delta/\Delta}$ embryos. An unpaired t-test was used to evaluate levels of Gli3FL and Gli3R and the Gli3R/Gli3FL ratio in four control and four*Inpp5e*$^{\Delta/\Delta}$ embryos derived from four different litters. (E-L) Formation of basal progenitors and neurons in the neocortex of *Inpp5e*$^{\Delta/\Delta}$ and *Inpp5e*$^{\Delta/\Delta}$;Gli3$^{\Delta699/+}$ embryos. In the lateral neocortex of E12.5 embryos, there is no significant difference in the proportions of Tbr1+ neurons (E, G, I, K) and basal progenitor cells (F, H, J, L) between control and *Inpp5e*$^{\Delta/\Delta}$;Gli3$^{\Delta699/+}$ embryos. Note the three bulges of the ventral telencephalon in *Inpp5e*$^{\Delta/\Delta}$;Gli3$^{\Delta699/+}$ embryos (J). Boxes indicate the regions where cell counts were performed. All statistical data are presented as means ± 95% confidence intervals (CI); unpaired t-tests (n=5) (B-D) and one way ANOVA followed by Tukey's multiple comparison test (K, L); * $p < 0.05$; ** $p < 0.01$; *** $p < 0.001$. Scale bars: 250μm (E), and 50μm (E'). bv: blood vessel; ctx: cortex.

Figure 8

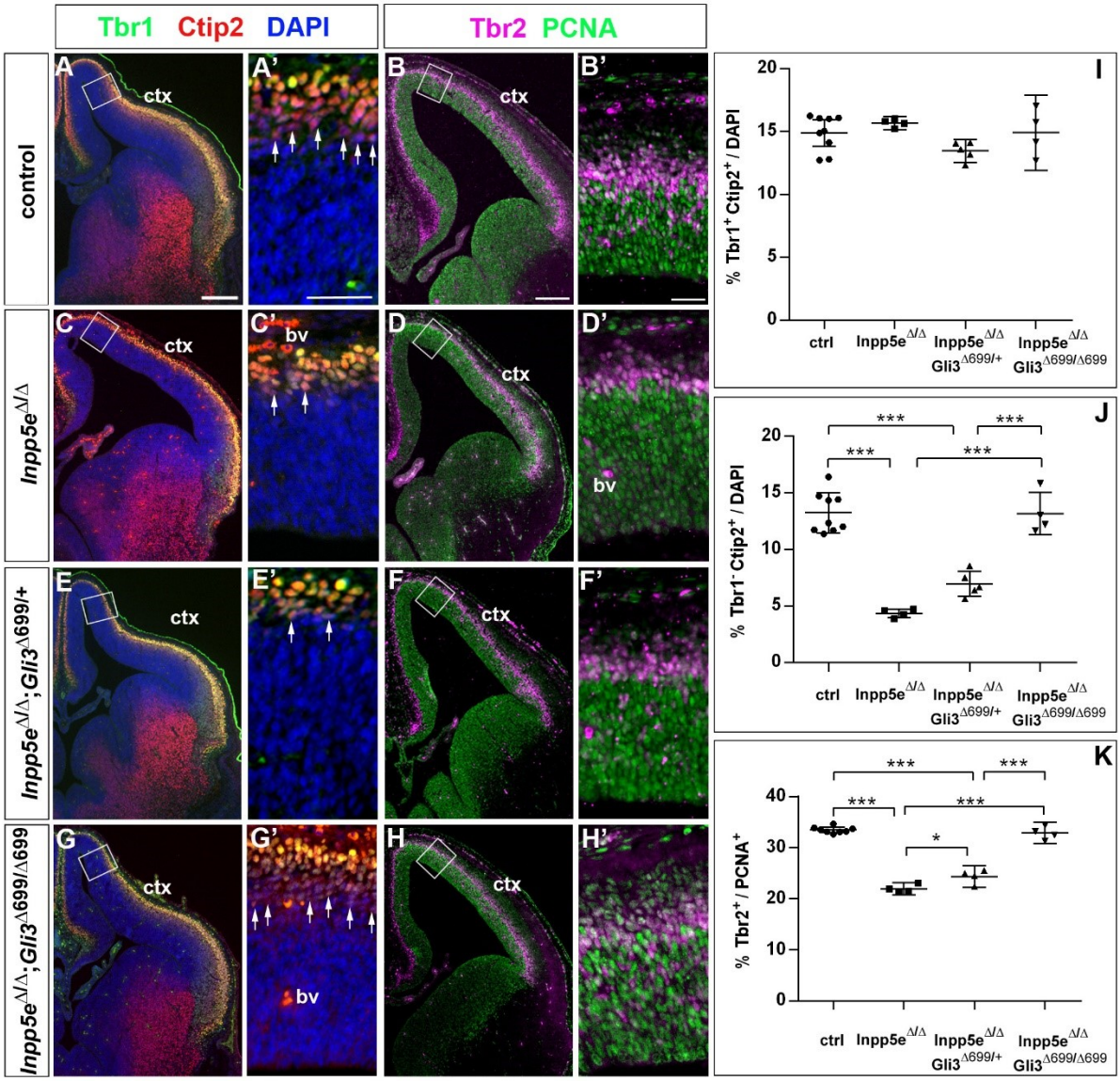

Figure 8: Two copies of the *Gli3* repressor allele are required to rescue the neurogenesis defects in E14.5 *Inpp5e* mutants. (A-H) Proportions of neurons (A, C, E, G) and basal progenitors (B D, F, H) in the medial neocortex of control, *Inpp5e*$^{\Delta/\Delta}$, *Inpp5e*$^{\Delta/\Delta}$;Gli3$^{\Delta699/+}$ and *Inpp5e*$^{\Delta/\Delta}$;Gli3$^{\Delta699/\Delta699}$ embryos. (A, C, E, G, J) The formation of Tbr1-Ctip2+ projection neurons is rescued after re-introducing two copies of the *Gli3* repressor allele. (B, D, F, H, K) The proportion of basal progenitors is slightly increased in *Inpp5e*$^{\Delta/\Delta}$;Gli3$^{\Delta699/+}$ embryos but a full rescue is only achieved in *Inpp5e*$^{\Delta/\Delta}$;Gli3$^{\Delta699/\Delta699}$ embryos. Boxes indicate the regions where cell counts were performed. All statistical data are presented as means ± 95% confidence intervals (CI); one way ANOVA followed by Tukey's multiple comparison test (I, J, K); * $p < 0.05$; *** $p < 0.001$. Scale bars: 250μm (A, B), 50μm (A', B'). bv: blood vessel; ctx: cortex.

Figure 9

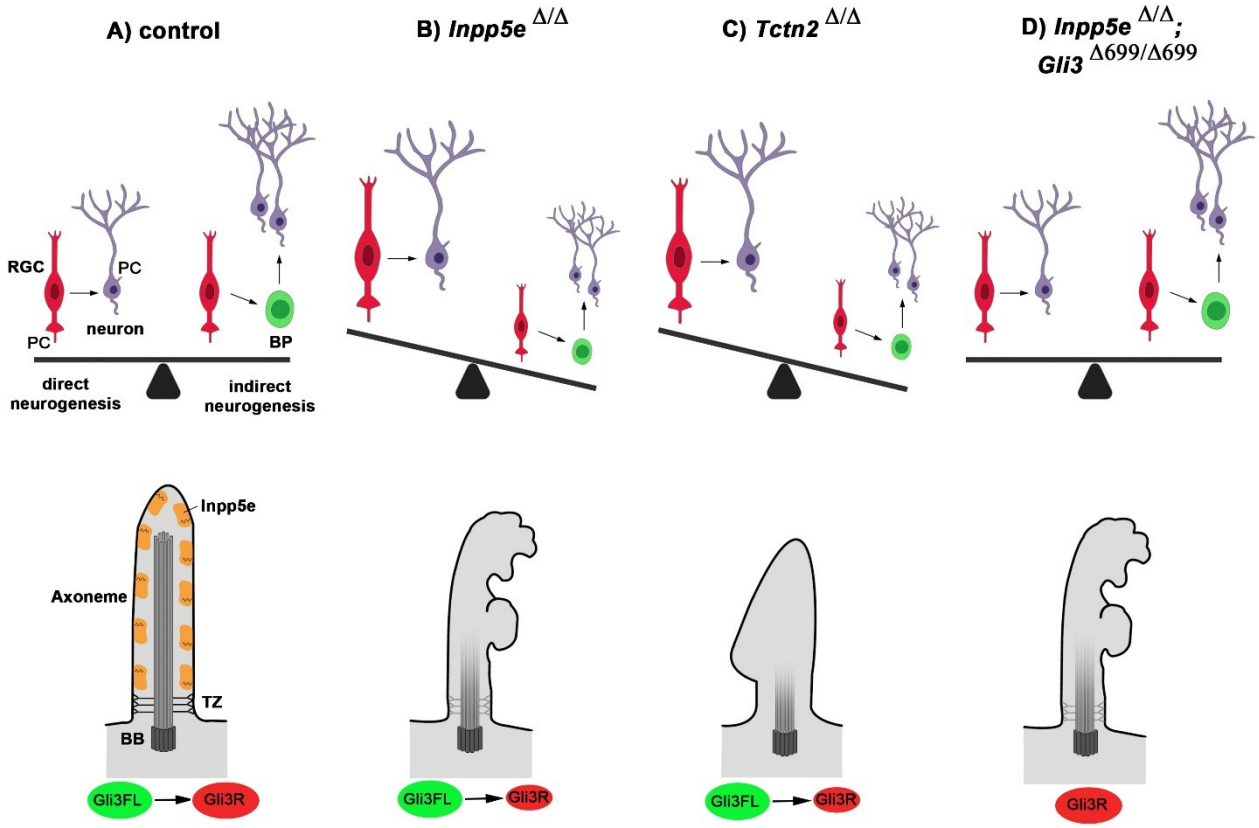

Figure 9: Model for *Inpp5e*'s role in controlling direct vs indirect neurogenesis in the developing cortex. (A) A fine-tuned balance between direct and indirect neurogenesis is required to produce cortical neurons in appropriate numbers. The structure of a primary cilium and the ciliary localisation of the Inpp5e protein are schematically indicated. (B) The *Inpp5e* mutation affects the axoneme (shaded microtubules) and ciliary morphology and may compromise the transition zone as indicated by the grayish colour (Dyson et al., 2017). Gli3R levels are reduced and there is a shift towards direct neurogenesis. (C) *Tctn2*$^{\Delta/\Delta}$ embryos have morphologically abnormal cilia, a defective axoneme and transition zone (Garcia-Gonzalo et al., 2011), lack ciliary Inpp5e protein (Garcia-Gonzalo et al., 2015) and phenocopy the neurogenesis defect of *Inpp5e*$^{\Delta/\Delta}$ mutants. (D) Introducing Gli3R in an *Inpp5e* mutant background restores Gli3 levels and the balance between direct and indirect neurogenesis. BB: basal body; BP: basal progenitor; PC: primary cilium; RGC: radial glial cell; TZ: transition zone.

Figure 1 - figure supplement 1

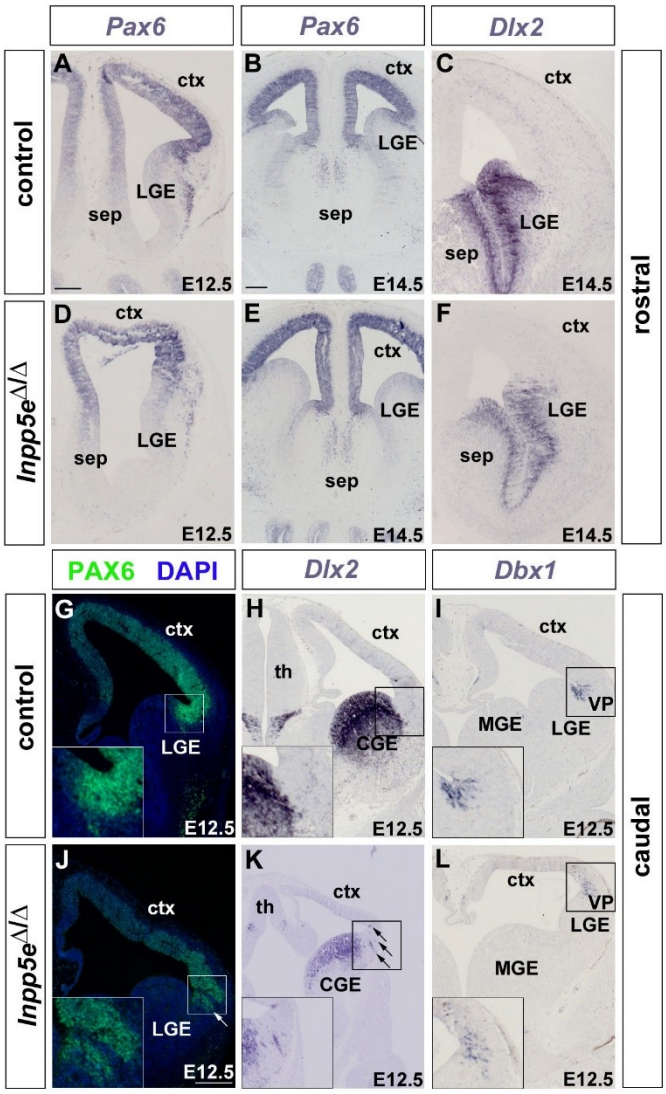

946

947 **Figure 1-figure supplement 1: Formation of the telencephalic boundaries in *Inpp5e*$^{\Delta/\Delta}$**
948 **embryos.** (A-F) Formation of the corticoseptal boundary. Expression of the dorsal marker gene *Pax6*
949 (A, B, D, E) and of the ventral marker gene *Dlx2* (C, F) remain restricted to the cortex and septum,
950 respectively, with a sharp expression boundary between both tissues. (G-L) Formation of the
951 pallial/subpallial boundary. While there is a sharp expression boundary between cortex and lateral
952 ganglionic eminence (LGE) in wild-type embryos (G-I), scattered Pax6 and *Dlx2* expressing cells
953 (arrows in J and K) are found in the mutant LGE and cortex, respectively, while the *Dbx1* expression
954 domain characteristic of the ventral pallium (VP) is fuzzier (L). CGE: caudal ganglionic eminence;
955 ctx: cortex; MGE: medial ganglionic eminence; sep: septum; th: thalamus. Scale bars: 200μm.
956

Figure 1 - figure supplement 2

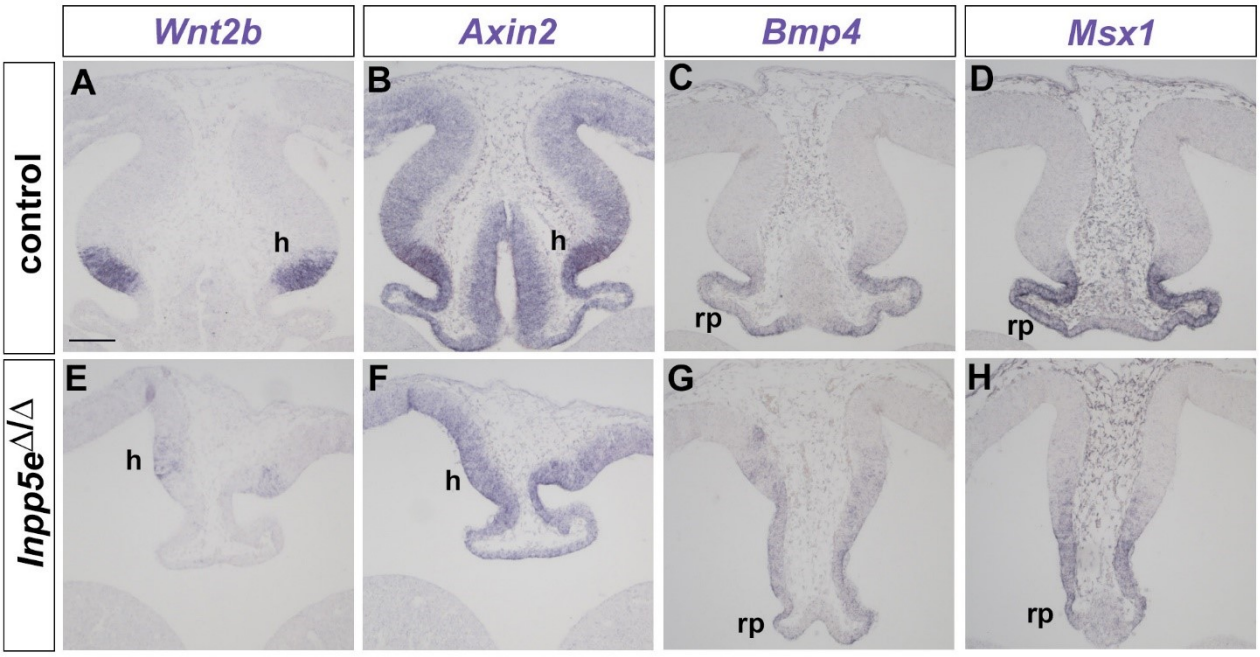

957

958 **Figure 1-figure supplement 2: Wnt/β-catenin and Bmp signalling in the dorsomedial**
959 **telencephalon of E12.5 *Inpp5e*$^{\Delta/\Delta}$ embryos.** (A, B, E, F) Reduced Wnt/β-catenin signalling in
960 *Inpp5e*$^{\Delta/\Delta}$ embryos. (A, E) *Wnt2b* expression is confined to the cortical hem (h) while there are only
961 few scattered Wnt2b expressing cells in the mutant. (B, F) Graded expression of the Wnt target gene
962 *Axin2* in the dorsal midline is reduced in mutant embryos. (C, D, G, H) Roof plate (rp) expression of
963 *Bmp4* and its target gene *Msx1* are reduced in *Inpp5e*$^{\Delta/\Delta}$ embryos. Scale bar: 100μm.

964

965

Figure 1 - figure supplement 3

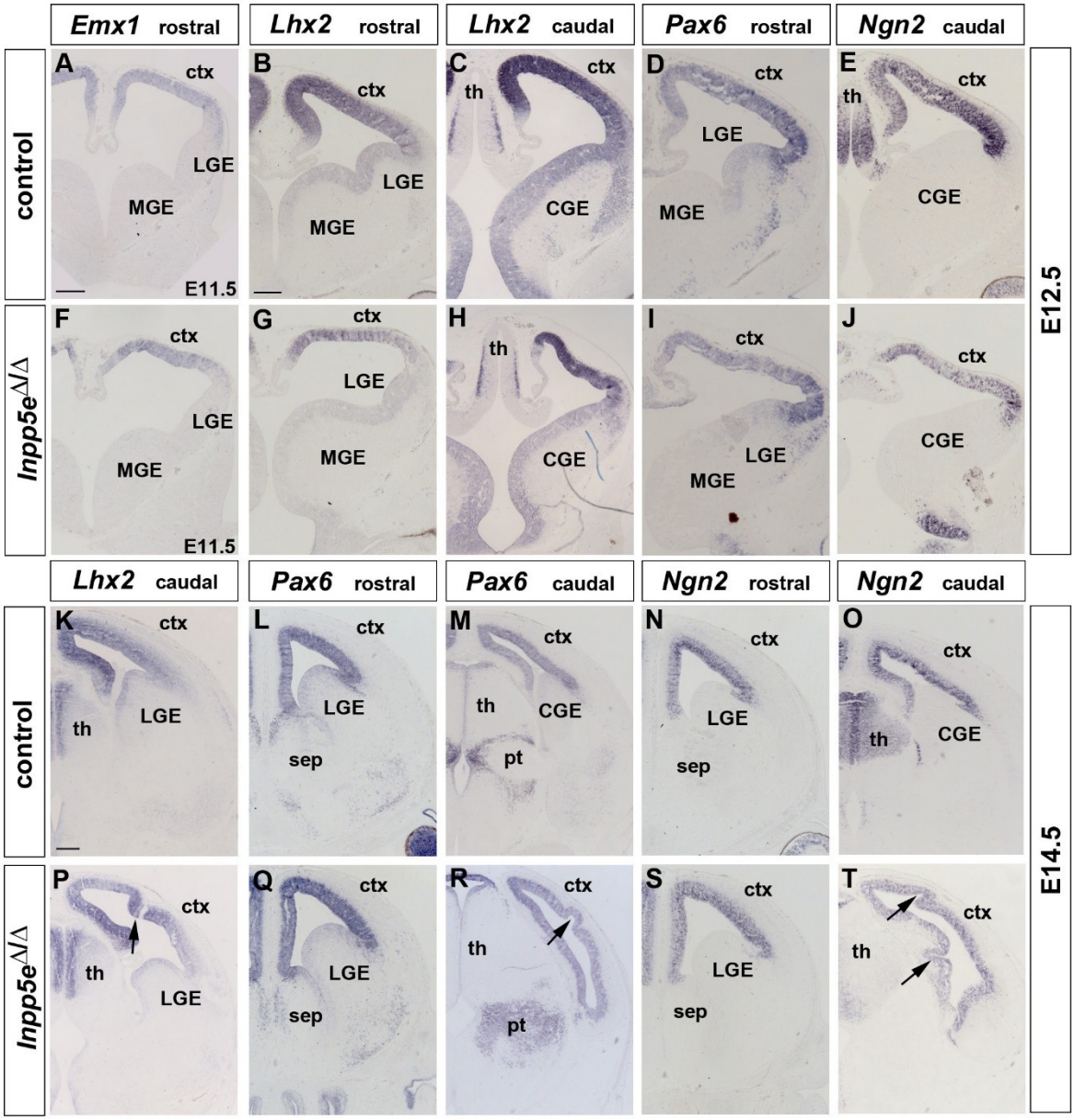

966

967 **Figure 1-figure supplement 3: Supplementary Figure 3: Expression of cortical progenitor**
968 **markers in *Inpp5e*$^{\Delta/\Delta}$ embryos.** (A-J) Dorsal marker gene expression at patterning stages (E12.5).
969 *Emx1*, *Lhx2*, *Pax6* and *Ngn2* are still expressed in the developing neocortex of *Inpp5e*$^{\Delta/\Delta}$ embryos
970 though the *Lhx2* medial to lateral (B, C, G, H) and the *Pax6*/*Ngn2* lateral to medial (D, E, I, J)
971 expression gradients are flatter. (K-T) Neocortical progenitors express *Lhx2*, *Pax6* and *Ngn2* in
972 E14.5 *Inpp5e*$^{\Delta/\Delta}$ embryos. Note the folding of the neocortex at caudal levels which occurs with 100%
973 penetrance (arrows in P, R and T). CGE: caudal ganglionic eminence; ctx: cortex; MGE: medial
974 ganglionic eminence; LGE: lateral ganglionic eminence; pt: prethalamus; sep: septum; th: thalamus.
975 Scale bars: 200μm.

976

Figure 3 - figure supplement 1

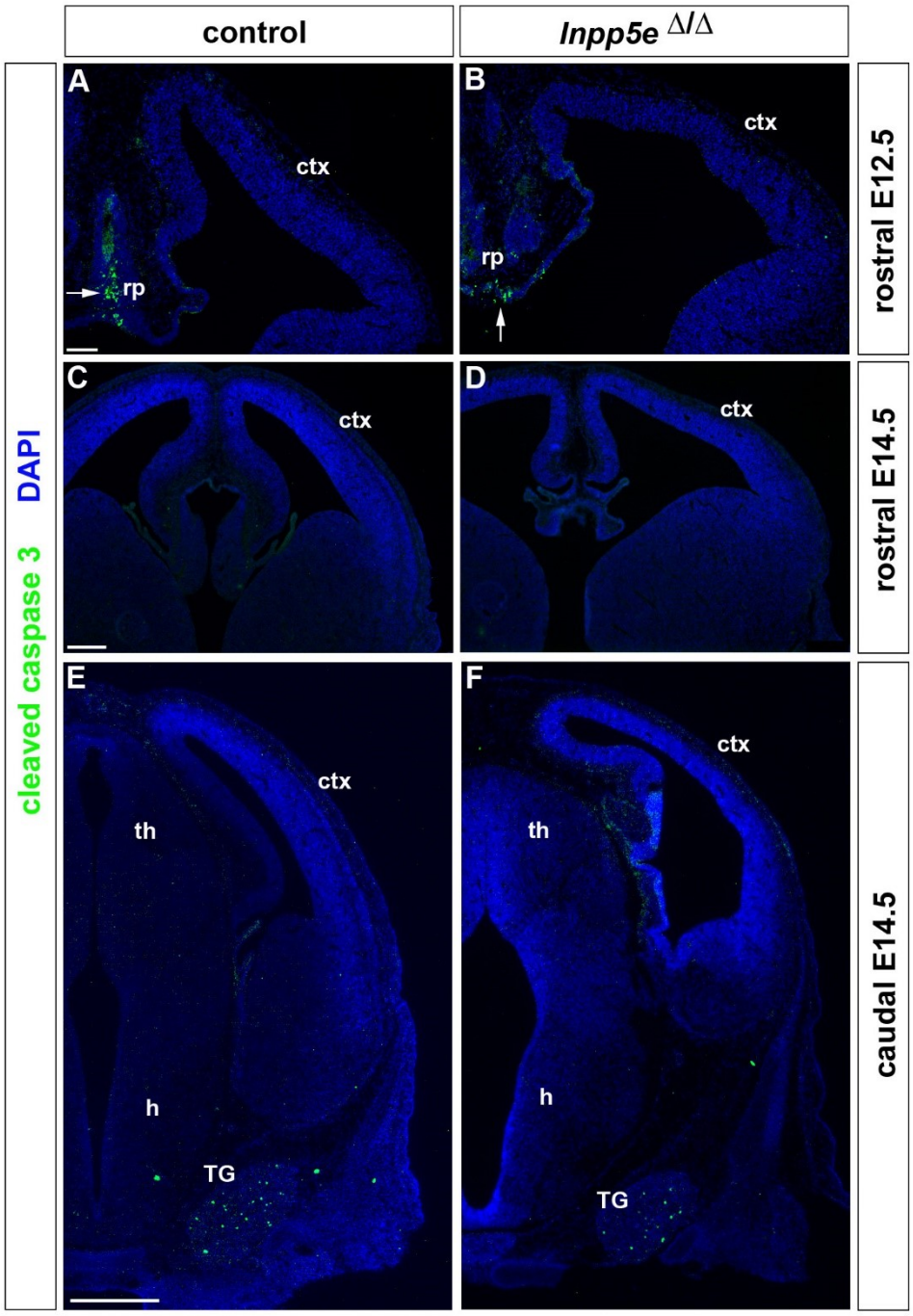

977

978 **Figure 3-figure supplement 1: Apoptosis in the developing forebrain of *Inpp5e*$^{\Delta/\Delta}$ embryos**. (A-
979 F) Immunofluorescence staining for Cleaved Caspase 3 revealing apoptic cells. (A, B) Programmed
980 cell death was detected in the midline roof plate (rp) but hardly in the developing neocortex of E12.5
981 control (A) and *Inpp5e*$^{\Delta/\Delta}$ embryos (B). (C-F) In E14.5 embryos, very few apoptotic cells were
982 identified in the neocortex while apoptosis is widespread in the trigeminal ganglion (TG) (E, F). ctx:
983 cortex. Scale bars: (A): 100μm, (C): 25`0μm, (D) 500μm.

Figure 3 - figure supplement 2

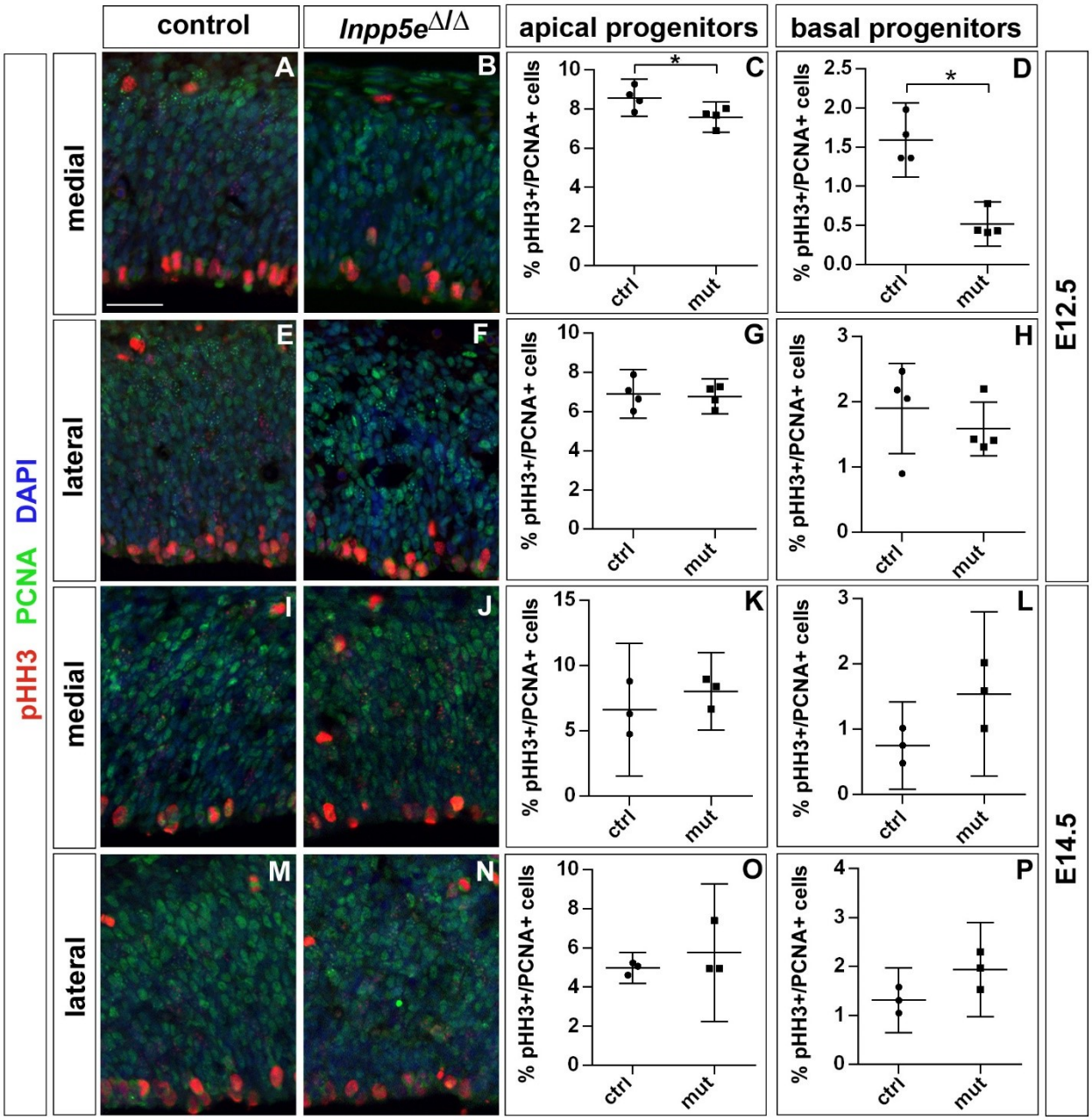

Figure 3-figure supplement 2: Proportion of mitotic progenitors in *Inpp5e*$^{\Delta/\Delta}$ embryos. (A-H) Proportions of mitotic progenitors in E12.5 control (A, E) and *Inpp5e*$^{\Delta/\Delta}$ embryos (B, F) as revealed by pHH3 (mitotic cells) and PCNA (all progenitor cells) double immunofluorescence. Note the reduction in mitotic basal progenitors in the *Inpp5e*$^{\Delta/\Delta}$ medial neocortex (A, B, D). (I-P) The proportions of apical and basal progenitors is not significantly different in E14.5 control and *Inpp5e*$^{\Delta/\Delta}$ embryos. In all panels, radial glia cells divide at the ventricular surface whereas mitotic basal progenitors locate in abventricular positions. All statistical data are presented as means ± 95% confidence intervals (CI); unpaired t-tests (C, G, K, L, P) and Mann Whitney tests (D, H, O); n = 4; * $p < 0.05$. Scale bar: 50μm.

Figure 3 - figure supplement 3

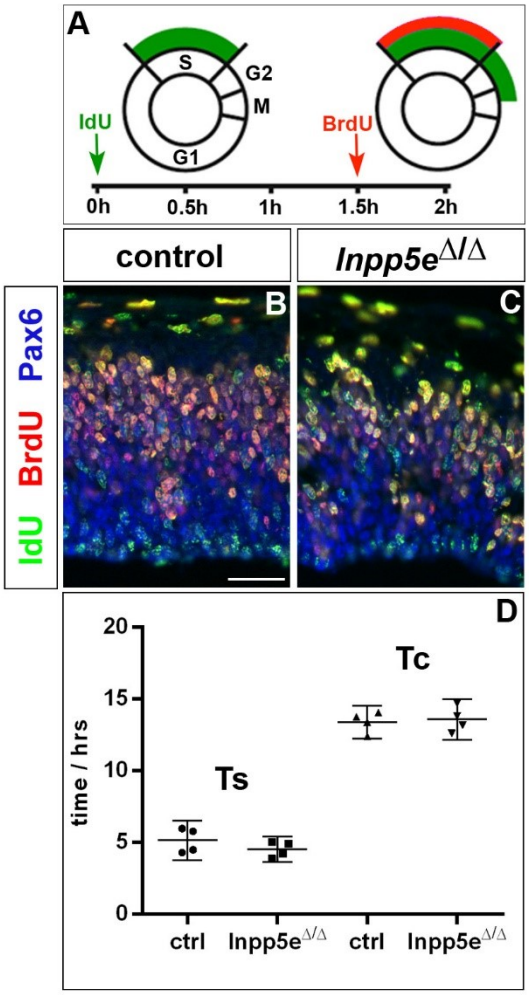

994

995 **Figure 3-figure supplement 3: Cell cycle of cortical progenitors in E12.5 *Inpp5e*$^{\Delta/\Delta}$ embryos.**
996 (A) Schematic illustrating the BrdU/IdU double labelling strategy to measure S phase (T_S) and total
997 cell cycle length (T_C). 90 minutes after an initial IdU administration, pregnant females received an
998 intraperitoneal BrdU injection. Embryos are harvested 30 minutes later. (B, C) Double
999 immunofluorescence to detect IdU+ and BrdU+ progenitors. (D) Quantification showing no significant
1000 change in T_S and T_C. Statistical data are presented as means ± 95% confidence intervals (CI);
1001 unpaired t-tests; n = 4; * $p < 0.05$. Scale bar: 50μm.

1002

Figure 4 - figure supplement 1

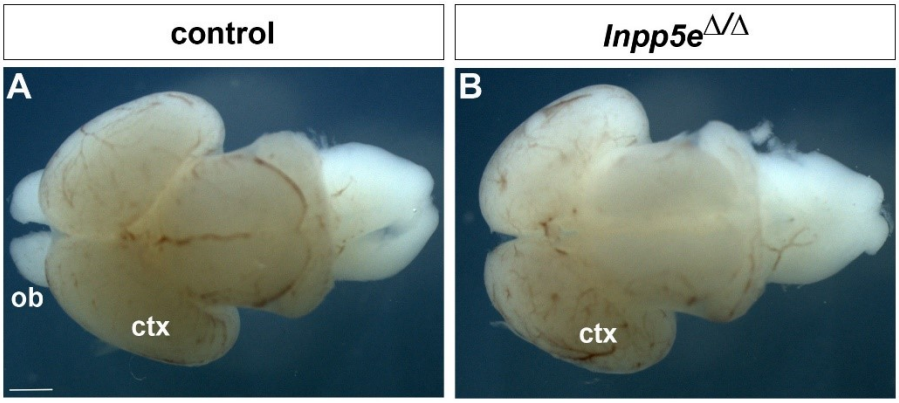

Figure 4-figure supplement 1: Whole mount preparations of E18.5 brains. (A) Control. (B) *Inpp5e*$^{\Delta/\Delta}$ brain. Note the absence of obvious protrusions of the olfactory bulbs (ob) in the mutant. Ctx: cortex. Scale bar: 1 mm.

Figure 4 - figure supplement 2

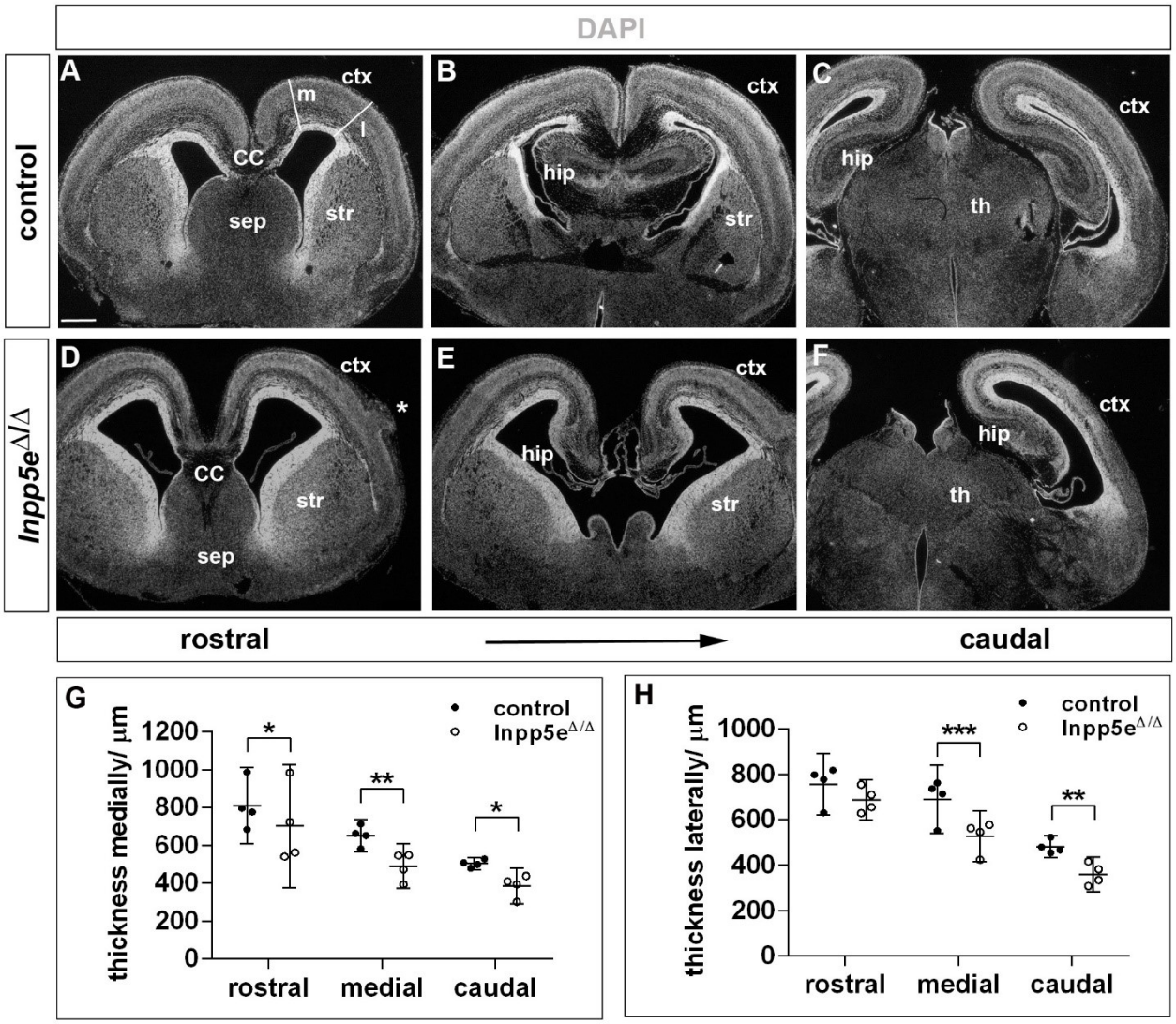

Figure 4-figure supplement 2: Forebrain malformations in E18.5 *Inpp5e*$^{\Delta/\Delta}$ embryos. (A-F) Coronal sections through the forebrain of E18.5 control (A-C) and *Inpp5e*$^{\Delta/\Delta}$ (D-F) embryos. The asterisk in (D) demarcates a heterotopia in the *Inpp5e* mutant. Note that the mutant lateral neocortex is thinner at most levels but not rostrolaterally (D- F). The lines in (A) indicate where cortical thickness was measured at medial (m) and lateral (l) levels. (G, H) Quantification of cortical thickness. CC: corpus callosum; ctx: cortex; hip: hippocampus; sep: septum; str: striatum; th: thalamus. Scale bar: 500µm. Statistical data are presented as means ± 95% confidence intervals (CI); Two way ANOVA followed by Sidak multiple comparisons test; n = 4; * $p < 0.05$; ** $p < 0.005$; *** $p < 0.001$.

Figure 4 - figure supplement 3

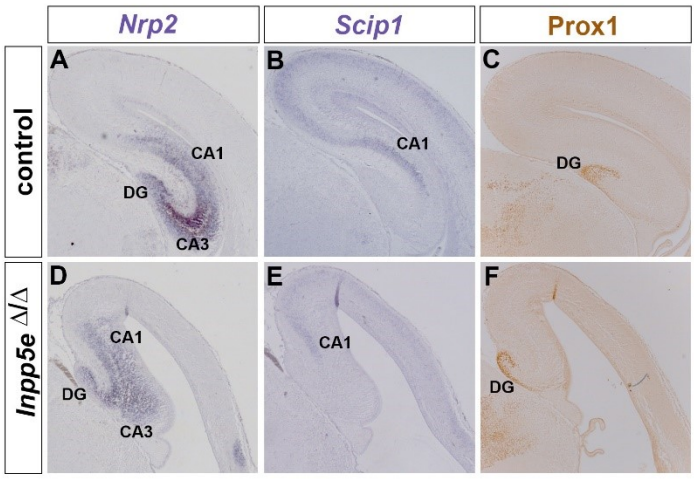

Figure 4-figure supplement 3: Hippocampus formation in *Inpp5e*$^{\Delta/\Delta}$ embryos. (A-F) Hippocampal marker gene expression in E18.5 control (A-C) and *Inpp5e*$^{\Delta/\Delta}$ embryos (D-F). Expression of *Nrp2* labels the whole hippocampal formation (*A*), while *Scip1* is expressed in CA1 and in the neocortex (*B*). Prox1 expression is confined to the dentate gyrus (DG) (*C*). In *Inpp5e*$^{\Delta/\Delta}$ embryos, these hippocampal markers are expressed but their expression domains are severely reduced or disorganized (*D-F*).

Figure 4 - figure supplement 4

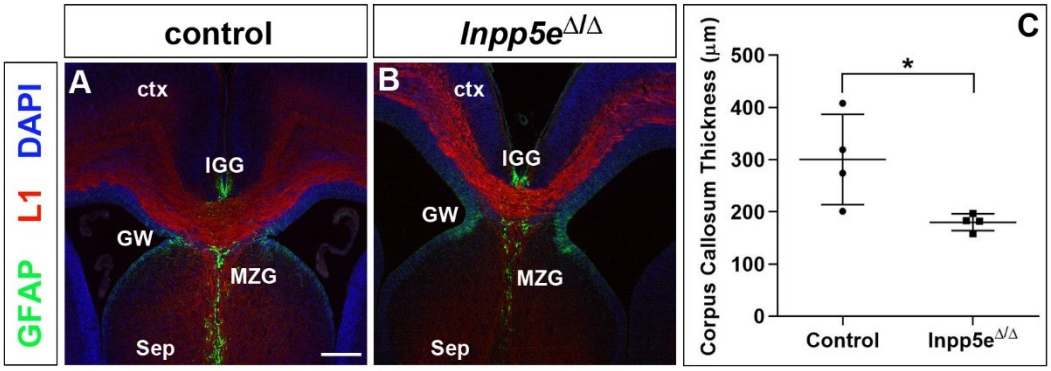

Figure 4-figure supplement 4: Formation of the corpus callosum in E18.5 *Inpp5e*$^{\Delta/\Delta}$ embryos. (A, B) Coronal section through the telencephalon stained with L1 and GFAP to reveal the corpus callosum (CC) and glial cells, respectively. The corpus callosum was smaller in *Inpp5e*$^{\Delta/\Delta}$ embryos while the glial wedge (GW), the induseum griseum glia (IGG) and the midline zipper glia (MZG) occupied their correct position surrounding the corpus callosum. (C) Quantification of corpus callosum thickness. Statistical data are presented as means ± 95% confidence intervals (CI); Mann-Whitney test; n = 4; * $p < 0.05$. Scale bar: 250μm.

Figure 7 - figure supplement 1

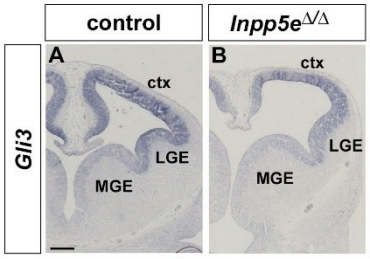

Figure 7-figure supplement 1: *Gli3* mRNA expression in Inpp5e mutants. (A, B) *Gli3* in situ hybridization showing *Gli3* mRNA expression in the cortex (ctx) and lateral ganglionic eminence (LGE) of control (A) and *Inpp5e*$^{\Delta/\Delta}$ embryos (B).

Figure 7 - figure supplement 2

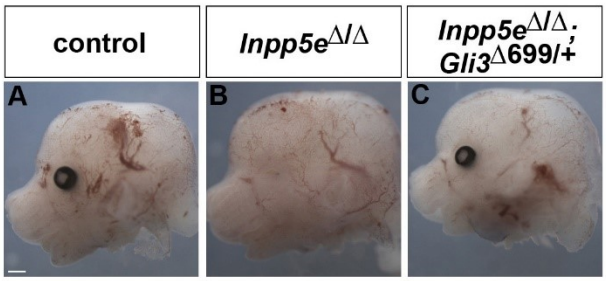

Figure 7-figure supplement 2: Rescue of eye development in *Inpp5e*$^{\Delta/\Delta}$;*Gli3*$^{\Delta699/+}$ embryos. (A-C) Side views of the heads of E12.5 embryos with the indicated genotype. *Inpp5e*$^{\Delta/\Delta}$ embryos lack the eye completely or only form a small remnant whereas eye formation is not affected in *Inpp5e*$^{\Delta/\Delta}$;*Gli3*$^{\Delta699/+}$ embryos. Scale bar: 1mm

Figure 7 - figure supplement 3

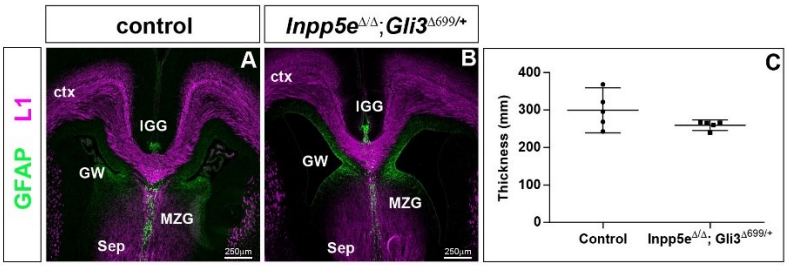

Figure 7-figure supplement 3: Rescue of corpus callosum formation in *Inpp5e*$^{\Delta/\Delta}$;*Gli3*$^{\Delta699/+}$ embryos. (A-B) Coronal section through the telencephalon stained with L1 and GFAP to reveal the corpus callosum (CC) and glial cells, respectively. There is no significant difference in the size of the corpus callosum between control and *Inpp5e*$^{\Delta/\Delta}$;*Gli3*$^{\Delta699/+}$ embryos; the glial wedge (GW), the induseum griseum glia (IGG) and the midline zipper glia (MZG) are formed in their correct position. (C) Quantification of corpus callosum thickness. Statistical data are presented as means ± 95% confidence intervals (CI); Mann Whitney tests; n = 4; Scale bar: 250µm.